pmod wrc

Annual Report 2009

Physikalisch-Meteorologisches Observatorium Davos und Weltstrahlungszentrum

Mission

Das PMOD/WRC

- dient als internationales Kalibrierzentrum für meteorologische Strahlungsmessinstrumente;
- entwickelt Strahlungsmessinstrumente für den Einsatz am Boden und im Weltraum;
- erforscht den Einfluss der Sonnenstrahlung auf das Erdklima.

Auftragerteilung

Das Physikalisch-Meteorologische Observatorium Davos (PMOD) beschäftigt sich seit seiner Gründung im Jahr 1907 mit Fragen des Einflusses der Sonnenstrahlung auf das Erdklima. Das Observatorium schloss sich 1926 dem Schweizerischen Forschungsinstitut für Hochgebirgsklima und Medizin Davos an und ist seither eine Abteilung dieser Stiftung. Auf Ersuchen der Weltmeteorologischen Organisation (WMO) beschloss der Bundesrat im Jahr 1970 die Finanzierung eines Kalibrierzentrums für Strahlungsmessung als Beitrag der Schweiz zum Weltwetterwacht-Programm der WMO. Nach diesem Beschluss wurde das PMOD beauftragt, das Weltstrahlungszentrum (World Radiation Center, WRC) zu errichten und zu betreiben.

Kerntätigkeiten

Das Weltstrahlungszentrum unterhält das Primärnormal für solare Bestrahlungsstärke bestehend aus einer Gruppe von hochpräzisen Absolut-Radiometern. Auf weitere Anfragen der WMO wurden 2004 das Kalibrierzentrum für Messinstrumente der atmosphärischen Langwellenstrahlung eingerichtet und 2008 das Kalibrierzentrum für spektrale Strahlungsmessungen zur Bestimmung der atmosphärischen Trübung. Seit 2007 wird auch das Europäische UV Kalibrierzentrum durch das Weltstrahlungszentrum betrieben. Das Weltstrahlungszentrum besteht heute aus vier Sektionen:

- Solare Radiometrie
- Infrarot Radiometrie
- Atmosphärische Trübungsmessungen (WORCC)
- Europäisches UV Kalibrierzentrum

Die Kalibriertätigkeit ist in ein international anerkanntes Qualitätssystem eingebettet (ISO 17025) um eine zuverlässige und nachvollziehbare Einhaltung des Qualitätsstandards zu gewährleisten.

Das PMOD/WRC entwickelt und baut Radiometer, die zu den weltweit genauesten ihrer Art gehören und sowohl am Boden als auch im Weltraum eingesetzt werden. Diese Instrumente werden auch zum Kauf angeboten und kommen seit langem bei Meteorologischen Diensten weltweit zum Einsatz. Ein globales Netzwerk von Stationen zur Überwachung der atmosphärischen Trübung ist mit vom Institut entwickelten Präzisionsfilterradiometern ausgerüstet.

Im Weltraum und mittels Bodenmessungen gewonnene Daten werden in Forschungsprojekten zum Klimawandel und der Sonnenphysik analysiert. Diese Forschungstätigkeit ist in nationale, insbesondere mit der ETH Zürich, und internationale Zusammenarbeit eingebunden.

Das PMOD/WRC ist eine Abteilung der Stiftung
Schweizerisches Forschungsinstitut für
Hochgebirksklima und Medizin in Davos.

Physikalisch-Meteorologisches Observatorium Davos
und World Radiation Center (PMOD/WRC)
Dorfstrasse 33
7260 Davos Dorf
Schweiz

pmod wrc

Annual Report 2009

Annual Report 2009

Table of Contents

3 Jahresbericht 2009

5 Introduction

6 Operational Services

6 Quality Management System
6 Calibrations
7 Solar Radiometry Section (WRC-SRS)
8 Infrared Radiometry Section (WRC-IRS)
9 Atmospheric Turbidity Section (WRC-WORCC)
10 Maintenance of the PFR Calibration Triad at WORCC
11 EUSAAR: Aerosol Optical Depth Inter-Comparison Campaigns
12 European Ultraviolet Calibration Center (EUVC)

13 Instrument Development

13 Instrument Sales
13 Solar Radiometry Section
14 A Finite Element Model for the Investigation of Thermal Properties of a PMO6 Type Radiometer
16 Space Experiments

18 Scientific Research Activities

18 Overview
19 Total Ozone Recovery and its Sensitivity to Different Forcing Factors
20 Changes of the Ozone Layer during the 21st Century
21 Response of the Middle Atmosphere to Short-Term Solar Irradiance Variability during Different Quasi-Biennial Oscillation Phases
22 Atmospheric Effects of an Extreme Solar Proton Event
23 Modeling of the Atmospheric Response to Mt. Pinatubo Eruption
24 Climate Engineering by Injection of Sulfate Containing Gases and its Implications for the Ozone Layer
25 Simulation of the Ozone Layer without Montreal Protocol Limitations
26 Sensitivity of the Earth's Middle Atmosphere to Short-Term Solar Variability and its Dependence on the Choice of Solar Irradiance Data Set
27 Nowcast of the Middle Atmosphere and Ionosphere State with the Chemistry-Ionosphere-Climate Model SOCOL^{i}
28 Effective Surface Albedo at Davos
29 Long-Term Trend Analysis of Cloud-Free Down-Welling Long-Wave Radiation from four Swiss Sites
30 NLTE Solar Irradiance Modeling with the COSI Code
31 The Shape of the Solar Limb
32 TSI and SSI Reconstruction back to the Maunder Minimum
33 Evidence of Solar Cycle Velocity Amplitude Changes Consistent with Mode Conversion Theory
34 Reconstruction of a Century of Broadband Atmospheric Transmission using Historic and Contemporary Pyrheliometer Measurements
35 PMO6-type Radiometer Calibration at the Total Solar Irradiance Facility at the Laboratory for Atmospheric and Space Physics in Boulder

36 Publications

36 Refereed Publications
38 Other Publications

39 Administration

39 Personnel Department
40 Guided Tours
41 Public Seminars
41 Course of Lectures, Participation in Commissions
41 Remission of Debts
42 Upgrading and Renovation of the Old Schoolhouse
43 Bilanz 2009 inklusive Drittmittel
43 Erfolgsrechnung 2009 inklusive Drittmittel

44 Abbreviations

Jahresbericht 2009

Werner Schmutz

Dienstleistungsbetrieb Weltstrahlungszentrum

Die Finanzierung des Weltstrahlungszentrums bleibt trotz der schwierigen finanziellen Situation der Gemeinde Davos stabil. Dabei ist es günstig, dass wir uns im Moment in der Mitte einer Vier-Jahres Vertragsperiode befinden und die Erneuerung der Vereinbarung erst dieses Jahr für die Periode 2012-2015 verhandeln werden muss. Wir sind zuversichtlich, dass eine Verlängerung gelingen wird, da die Dienstleistungen des Weltstrahlungszentrums mehr denn je gefragt sind. Wie schon für 2008 können wir erfreulicherweise auch für diese Berichtsperiode eine neue Rekordzahl von Kalibrierungen verzeichnen.

Der im Jahr 2008 entwickelte erste Prototyp zur genauen Messung der Himmels-Infrarotstrahlung (IRIS1) hat nun ein ganzes Jahr parallel zur Infrarot-Strahlungsreferenz gemessen, eine Gruppe von ausgewählten Pyrgeometer Instrumenten. Die Infrarot Standardgruppe ist nach wie vor in sich konsistent und stabil, weist aber gegenüber dem IRIS1 Instrument einen systematischen Jahresgang auf, dessen Ursache noch nicht sicher bestimmt ist. Wir vermuten, dass diese systematische Variation auf Transmissionseigenschaften der Dome der Pyrgeometer Instrumente zurückzuführen ist. Eine Bestätigung dieser Hypothese kommt vom neuen, im Grundprinzip etwas modifizierten zweiten Prototyp, IRIS2, der in Betrieb genommen wurde und der für das letzte halbe Jahr, für das Vergleichsdaten vorliegen, ausgezeichnet mit IRIS1 übereinstimmt.

Das von der WRC-Sektion für atmosphärische Trübung betreute Präzision-Filter-Radiometer (PFR) Netzwerk zur weltweiten Überwachung der Trübung bestand ursprünglich aus zwölf Messstationen. Das Messnetz wurde mittlerweile um neun assoziierte Stationen erweitert und umfasst nun 21 Messorte. Der Ausbau des Netzwerks betrifft vor allem Stationen in Nordeuropa.

Drei PFR-Instrumente dienen als Kalibrier-Referenz in Davos. Routinemässig wurde eines dieser Referenz-Instrumente ausgetauscht und die Kalibrierfaktoren der einzelnen Kanäle der Instrumente dieser Gruppe überprüft und geringfügig korrigiert. Im Rahmen des FP6 Projektes EUSAAR wurden Audits und Vergleichsmessungen bei drei PFR Stationen durchgeführt.

Das Europäische Ultraviolett Kalibrierzentrum hat mit dem Referenz-Spektroradiometer QASUME wiederum mehrere UV Messstationen besucht. Aussergewöhnlich war eine Vergleichs-Messkampagne auf Ny-Ålesund in Norwegen, an der neben QASUME zwei Spektroradiometer und vier UV-Filterradiometer von verschiedenen Europäischen Forschungsinstitutionen teilnahmen.

Entwicklung und Bau von Experimenten

Der Bau des kryogenen Radiometers CSAR (Cryogenic Solar Absolute Radiometer) ist eine Kooperation mit den Metrologie-Instituten National Physics Laboratory, England und METAS, Bern. Der Beitrag des PMOD/WRC ist die Entwicklung und Herstellung eines Monitors, der die Transmission des Fensters zum Vakuumtank, in dem das kryogene Radiometer betrieben wird, mit hoher Präzision während den Messungen bestimmt. Das langfristige Ziel ist, dass CSAR die Weltstandardgruppe, die die Weltstrahlungsreferenz repräsentiert, ersetzt. Das Projekt kommt erfreulich gut voran und wir erwarten wie geplant, dass wir CSAR für eine erste Mess-Demonstration während der kommenden elften Internationalen Pyrheliometer Vergleiche im Herbst 2010 in Betrieb nehmen können. Falls der Übergang von einem Artefakt als konventioneller Primärstandard zu einer Technologie-Realisation einer SI-rückführbaren absoluten Messung gelingt, wird dies für die solare Radiometrie ein gewaltiger Fortschritt sein.

Weltraumprojekte

Am 2. November 2009 wurde die ESA Technologie-Mission PROBA2 erfolgreich gestartet. Mit an Bord ist LYRA, ein Experiment, welches in vier verschiedenen UV Spektralbereichen mit hoher zeitlicher Auflösung die Sonnenstrahlung misst. Erstmals im Weltraum wurden Diamantsubstrat-Photodetektoren eingesetzt. Das Belgisch-Schweizerische Instrument wurde am Physikalisch-Meteorologischen Observatorium Davos und Weltstrahlungszentrum (PMOD/WRC) entwickelt und hergestellt. Die wissenschaftliche Führung unterliegt dem Belgischen Meteorologieinstitut Observatoire Royal de Belgique und die Gesamtprojektleitung erfolgte durch das Centre Spatial de Liège, Belgien. ‘First Light’, das erste Mal Sonnenlicht auf den Detektoren, erfolgte am 6. Januar 2010. Während der Inbetriebnahme konnte LYRA bereits erste kleinere Sonneneruptionen nachweisen. Es wird erwartet, dass LYRA/PROBA2 neue Erkenntnisse in der Erforschung der Sonneneruptionen liefert und die annähernd permanente Beobachtung der Ultraviolett-Sonnenstrahlung einen wesentlichen Beitrag zur „Space Weather“ Beurteilung ermöglicht.

Das zweite vom Observatorium Davos gebaute und abgelieferte Experiment ist PREMOS für die französische Mission PICARD. Während den Tests im Sommer 2009 zeigte sich, dass sich eines der zwei Absolut-Radiometer nicht mehr einwandfrei verhielt. Das ganze Experiment PREMOS wurde im August zurück ans Observatorium gebracht und das fehlerhafte Instrument durch ein Ersatzinstrument ausgetauscht. Da das Ersatzinstrument vorgängig sowohl am NPL in London als auch am LASP in Boulder kalibriert worden ist, bringt dieser Austausch eine weitere Rückführbarkeit der mit PREMOS gemessenen Strahlung zur SI-Skala. Im September konnte PREMOS wieder auf PICARD integriert werden und im Dezember bestand das Experiment alle Tests. Der Start von PICARD ist für den 15. Juni 2010 vorgesehen.

Klimaforschung

Die Klimagruppe des PMOD/WRC hat mit SOCOL, dem am PMOD/WRC entwickelten Chemie-Klima-Modell, ein 140 Jahre langes Zeitintervall von 1960 bis ins Jahr 2100 simuliert. Dabei wurden vorausgesagte Szenarien für die Entwicklung der Treibhausgase und der Temperatur als Randbedingung

angenommen. Es konnten verschiedene Schlussfolgerungen bezüglich der zu erwartenden Veränderungen der Ozonschicht gezogen werden. Die Resultate werden unter anderem auch in den nächsten WMO Report zum Status der Ozonabnahme einfliessen.

Für das FP7 Projekt SOTERIA ist unser Beitrag eine Jetzt-Prognose der chemische Zusammensetzung der mittleren Atmosphäre. Zur weiteren Vorbereitung dieser Aufgabe haben wir verschiedener Einflüsse auf das Verhalten der Modellresultate untersucht. Da wir nun im Wesentlichen die Vorbereitungsarbeiten abgeschlossen haben, sollte bald nach dem regelmässigen Eintreffen der LYRA/PROBA2 Daten – das sollte ab Mitte 2010 geschehen – unser Versuchsbetrieb eines operationellen „Now-cast" mit nur rund einer Stunde Verzögerung via Internet abrufbar werden.

Theoretisch erwartet man einen direkten Zusammenhang zwischen der Zunahme der Bodentemperaturen und der spezifischen Luftfeuchte mit der atmosphärischen Infrarot Himmelsstrahlung. Eine Untersuchung der Trends der IR Strahlung anhand von Beobachtungen in der Schweiz, gemittelt über Monate, zeigt tatsächlich den erwarteten Zusammenhang: Die IR Strahlung nahm in den letzten 15 Jahren zu. Die Trends der IR Monats-Strahlungsmittel sind in allen Monaten, ausser im August im Frühling, Sommer und Herbst positiv. Überraschenderweise nimmt die IR Strahlung aber im Winter ab. Statistische Analysen zeigen allerdings, dass noch keine der Trends innerhalb von 95 % Wahrscheinlichkeit signifikant sind.

Personelles

Vier neue Mitarbeiter kamen im Berichtsjahr ans Observatorium Davos und da uns niemand verlassen hatte, verzeichnete das Institut Ende 2009 eine Rekordzahl von Mitarbeitern: Es waren 36 Personen am PMOD/WRC angestellt. Mit dem Eintritt von Daniel Lachat haben wir nun sechs Doktoranden. Die Gruppe, die unsere Weltraumexperimente entwickelt, wurde durch Markus Suter erweitert, der uns schon aus seiner Zeit als Zivildienstleistender bekannt war. Marco Senft, den wir zur Programmierung der neuen Datenerfassung temporär eingestellt haben, betreute bisher als externer Beauftragter unsere IT-Infrastruktur.

Im Oktober kam Peter Kiedron vom NOAA, Boulder, als Gastwissenschaftler zu uns. Er ist im Rahmen des von der Innovationsstiftung des Kantons Graubünden geförderten Entwicklung eines neuen Spektroradiometers temporär angestellt. Wir sind sehr erfreut, dass wir diese Position mit einem Wissenschaftler besetzen konnten, der langjährige Erfahrung in der Entwicklung solcher Instrumente mitbringt.

Infrastruktur

Während der Bausaison 2009 wurde auf der Westseite des Alten Schulhauses eine Nottreppe mit einem integrierten Lift erstellt. Hinter der Werkstatt wurde eine Zufahrt angelegt, mit der wir nun via neuem Lift einen stufenlosen Zugang zu allen Stockwerken des Gebäudes haben. Die Arbeiten konnten 2009 noch nicht vollständig abgeschlossen werden und der Anbau wird daher erst im Frühjahr 2010 fertig gestellt sein. Im Jahr 1999, als ich meine Tätigkeit am PMOD/WRC begann, war die Mitarbeiterzahl ungefähr die Hälfte der Personen, die wir heute beschäftigen. Diese Expansion hat allen verfügbaren Platz im Alten Schulhaus beansprucht und daher haben wir vor zwei Jahren begonnen, die Umstrukturierung und den weiteren Ausbau der Raumreserven zu planen. Das Bundesamt für Bauten und Logistik hat die Firma Emch+Berger AG mit der Gesamtplanung beauftragt. Die Planungsphase ist nun mit der Eingabe der Baupläne bei der Davoser Baubehörde abgeschlossen worden. Der Umbau wird vor allem eine Erschliessung des vierten Stocks bringen, in dem ein grösserer Seminarraum untergebracht wird. Dieser wird genügend Kapazität bieten, um die Teilnehmer der wiederkehrenden Internationalen Pyrheliometer Vergleiche aufzunehmen. Die Erweiterung und Neuaufteilung ermöglicht aber auch Platz für rund zehn zusätzliche Arbeitsplätze und im Untergeschoss wird ein weiteres Optiklabor integriert werden. Wir haben besonders darauf geachtet, dass das Äussere des Hauses möglichst minimal beeinträchtigt wird, da das Gebäude ein historischer Zeitzeuge an exponierter Lage ist. Die einzige von aussen sichtbare Änderung wird auf der Nordseite die Aufstockung des Zwerchhauses sein, in dem das Treppenhaus untergebracht ist und das dann zwei weitere Stockwerke erschliessen wird. Die repräsentative Südseite, die der Stadt Davos zugewandt ist, bleibt unverändert. Dieser rücksichtsvolle Umgang mit der historischen Bausubstanz wurde vom Architekturbüro Schumacher AG entworfen. Die Kosten des Umbaus werden vollständig vom Bund übernommen. Der Baubeginn wird im Oktober 2010 sein.

Dank

Dem Bund gebührt zweifacher Dank: Einerseits hat er den Bau der Nottreppe, des neuen Lifts und der Zufahrtsstrasse alleine, ohne die beiden Finanzierungspartner des Weltstrahlungszentrums, Kanton Graubünden und Gemeinde Davos, bezahlt. Andererseits hat der Bundesrat im letzten Jahr auch entschieden, dass er für das PMOD/WRC den Anteil am Fehlbetrag der ehemaligen Pensionskasse des Bundes beim Übertritt in die PUBLICA übernimmt. Zusammen machen diese beiden Beiträge über CHF 870'000.00 zusätzliche Einnahmen aus, die dem Observatorium zu Gute kamen. Der Fehlbetrag, den wir über viele Jahre transitorisch bereitgestellt hatten, fliesst in unsere Rückstellungen, die es ermöglichen werden, nach dem Umbau in die Neuausrüstung der Infrastruktur zu investieren.

Dem Präsidenten und den Mitgliedern des Ausschusses des SFI sowie dem Präsidenten und den Mitgliedern der Aufsichtskommission WRC danke ich für ihre gute und unterstützende Begleitung der Institutsaufgaben. Die Grundfinanzierung des WRC ist dem Bund, dem Kanton Graubünden und der Gemeinde Davos zu verdanken.

Die Mitarbeiter des Observatoriums haben wesentlich dazu beigetragen, dass das Jahr 2009 positiv abgeschlossen werden konnte. Ich danke ihnen aber nicht nur für den monetären Erfolg, sondern mein herzlicher Dank gilt vor allem den vielen wertvollen Beiträgen in der Instrumentenentwicklung und in der Forschung, die zum guten Ruf unseres Institutes beitragen.

Introduction

Werner Schmutz

The funding situation of the PMOD/WRC operational services remains stable despite the difficult financial status of the Davos community. It is beneficial that we are now mid-term of the four-year contract. The renewal of the contract for the funding of the World Radiation Center needs to be agreed next year between the Davos local authority, the Kanton Graubünden, and the Swiss federal government for the 2012 to 2015 funding period. We are confident that a continuation will be possible as the operational services are in higher demand than ever. Similar to 2008, we are again happy to report that our calibration service achieved a new record number of calibrations in 2009.

Towards the end of last year, the ESA PROBA2 technology mission was successfully launched on November 2, 2009. One of the experiments on board is LYRA. The LYRA PI institute is the Royal Observatory of Belgium which contributed the novel diamond detectors. LYRA consists of four large pass band channels where each channel observes solar irradiance in the soft X-ray or UV pass bands. Their exact choice was made with regard to addressing scientific questions in Solar Physics, Aeronomy, and Space Weather. LYRA weighs 3.53 kg, and measures 315 mm x 92.5 mm x 222 mm. The hardware and electronics were designed and manufactured in-house at PMOD/WRC. LYRA "First light" was on January 6, 2010 and it successfully passed the commissioning phase. After several days, the instrument observed its first solar flares with an unprecedented high time resolution of 0.5 sec. LYRA will soon be operating nominally and its data will be used in research studies and for space weather forecasts.

Another highlight is the development of a Cryogenic Solar Absolute Radiometer (CSAR) to measure solar irradiance which is progressing very well. This project is a collaboration with the two metrology institutions National Physics Laboratory, England and METAS, Bern. The PMOD/WRC contribution is the development of a monitor to determine the transmittance of the entrance window to the vacuum tank containing the radiometer with high precision. The goal of CSAR is to replace the World Standard Group, which represents the World Radiometric Reference, in the mid-term future by a more precise SI traceable technology realization of the absolute measurement of the irradiance. This will represent a major advancement in radiometry, and given the PMOD/WRC operational service contract, it will be its major new facility. We are looking forward to implementing CSAR for a first technology demonstration at the next IPC-XI in autumn 2010 at Davos.

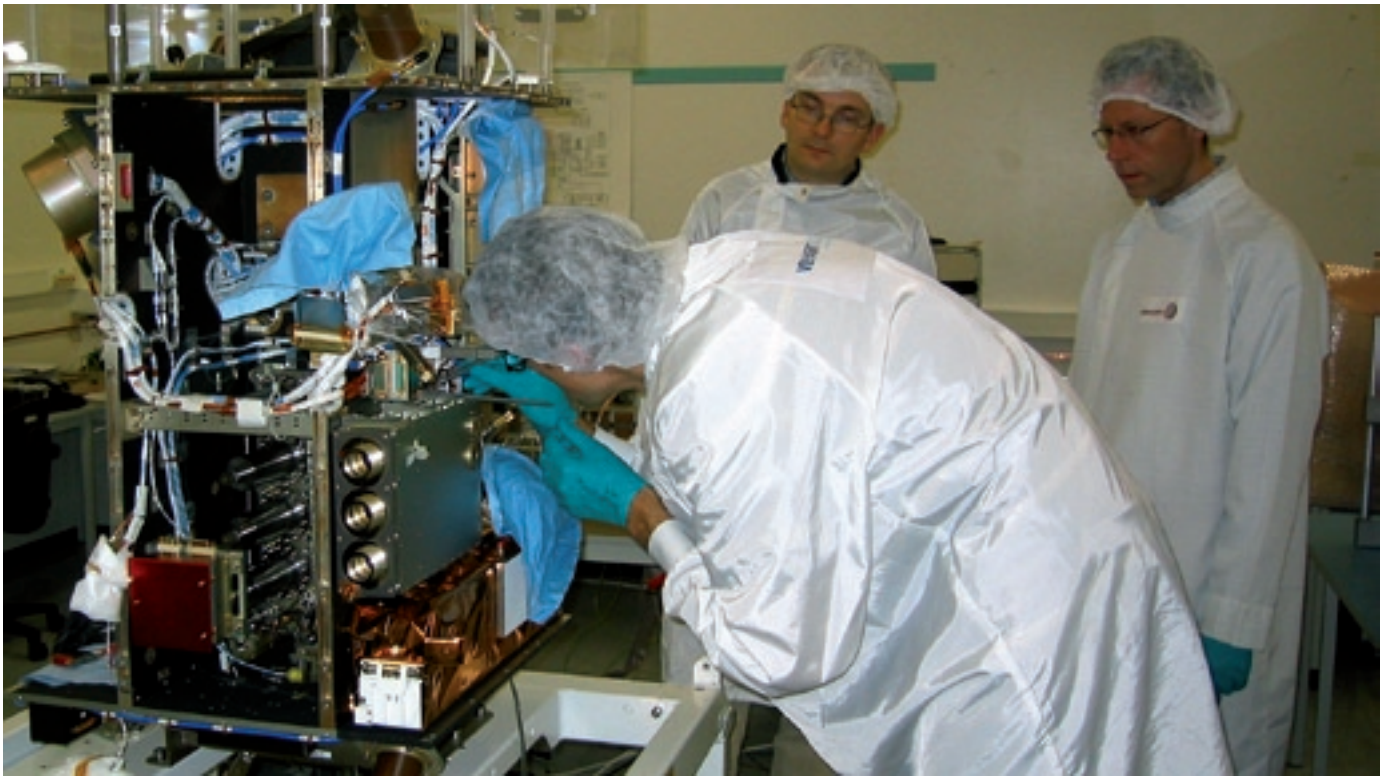

Figure 1. Integration of LYRA on the spacecraft PROBA 2 on March 5, 2007 at the Belgian firm Verhaert Space. The person to the right is Silvio Koller, observing critically the mounting procedure. He was LYRA instrument engineer at PMOD/WRC and was responsible for all manufacturing aspects of the hardware and electronics.

Operational Services

Quality Management System

Silvio Koller

PMOD/WRC QMS

Since 2006 the PMOD/WRC maintains an approved quality management system based on the general requirements for the competence of testing and calibration laboratories (EN ISO/IEC 17025).

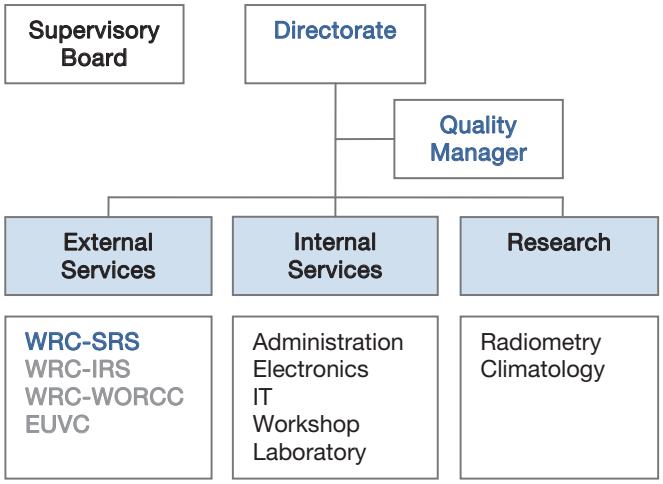

Figure 1. Organizational chart of the PMOD/WRC quality management system. The WRC Solar Radiometry Section performs its calibrations according to the EN ISO/IEC standard 17025.

To date, the WRC Solar Radiometry Section is covered by the QMS and it calibrates customer instruments in accordance to the EN/ISO standard.

PMOD/WRC is a designated institute of the Swiss National Metrology Institute, METAS, which is signatory of the CIPM-MRA (Comité international des poids et mesures - Mutual Recognition Arrangement).

Quality Management System Activities

Two calibration and measurement capabilities (CMC) are listed in the database of the „Bureau International des poids et mesures“ (BIPM): Responsivity, direct and global solar irradiation.

Inter-laboratory comparisons were performed at NREL in Golden, CO using two WRR traceable transfer standards (PMO6 and AHF) during NPC2009.

A 3-Laboratory comparison in power mode (NPL-NIST-WRC) and WRR to NIST traceable irradiance measurements were performed with PMO6 type radiometers at LASP, Boulder CO.

Calibrations

Silvio Koller

Solar Radiometry Section (WRC-SRS)

The total number of instrument calibrations within this section increased again in 2009 to the remarkable number of 100. The WRC section „Solar Radiometry“ calibrated 77 pyranometers, 6 pyrheliometers and 17 actinometers during 87 days of measurement.

Infrared Radiometry Section (WRC-IRS)

The infrared radiometry section of the World Radiation Center calibrated 22 Pyrgeometers in 2009. The calibration procedure consists of characterization with a black-body source and direct outdoor comparison of downwelling longwave irradiance against the World Infrared Standard Group (WISG) of pyrgeometers.

Atmospheric Turbidity Section (WRC-WORCC)

The World Optical depth Research and Calibration Center calibrated 11 Precision Filter Radiometers by comparison to the WORCC standard Triad. Four of these PFR belong to the GAW network, and seven to international institutes.

European Ultraviolet Calibration Center (EUVC)

The Ultraviolet Calibration Center of the PMOD/WRC calibrated five spectroradiometers at their respective field sites using the traveling reference spectroradiometer QASUME.

Six UVB, one UVB/UVA broadband radiometer and two multi-channel radiometers were calibrated.

In September 2009, 17 Brewer spectrophotometers were calibrated relative to the QASUME spectroradiometer during the 4th RBCC-E campaign at El Arenosillo, Spain.

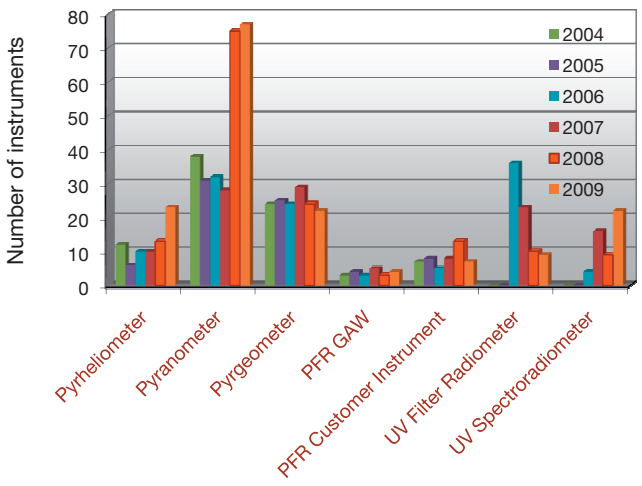

Figure 1. Statistics of instrument calibrations at PMOD/WRC.

Solar Radiometry Section (WRC-SRS)

Wolfgang Finsterle

Apart from offering calibration services the WRC-SRS was also engaged in improving and disseminating of its primary standard, the WRR. Renewal of some of the WRC technical facilities has started in 2009. The participation in radiometer comparison campaigns not only provides these events with the necessary traceability to the WRR but is also important to check the stability of the World Standard Group (WSG) which represents the WRR.

In 2009, the WRC-Solar Radiometry Section (WRC-SRS) participated in the U.S. National Pyrheliometer Comparison (NPC2009) again. The NPC2009 was organized by the National Renewable Energy Laboratory (NREL) in Golden, Colorado between 28 September and 1 October 2009. Two of our transfer instruments (PMO6-cc 0401 and AHF32455) participated in the comparisons to provide WRR traceability for some 30 cavities from the U.S.A. and Canada. These annual intercomparisons are also important for early recognition of potential stability problems with the WSG.

Stability checks are particularly valuable with regard to the old age of most of the radiometers which constitute the WSG. In 2009, the WSG was again not problem-free. Not only has the HF18748 continued to read low, but in August the amplifier for the PAC3 thermopile signal failed and was not repairable. In addition, the TMI MK67814 has been reading high since December. However, the HF18748 appears to have recovered and seems to be measuring correct again since October. Although no indication for a drift of the WRR has been found so far, these events clearly indicate that maintaining the stability of the WRR will become increasingly problematic in the future and the implementation of the Cryogenic Solar Absolute Radiometer (CSAR) during 2010 will be highly appreciated.

In addition, a new data acquisition system hardware was bought in 2009 consisting of two PXI compatible racks which hold a total of 16 digital multimeters (DMMs). These replace the current data acquisition system and roughly double the number of instruments that can be calibrated at any one time. This extension of capacity was becoming necessary to cope with the increasing number of calibration requests, which are mainly for pyranometers (see Section „Operational Services“).

Figure 1. NPC 2009 in Golden, Colorado.

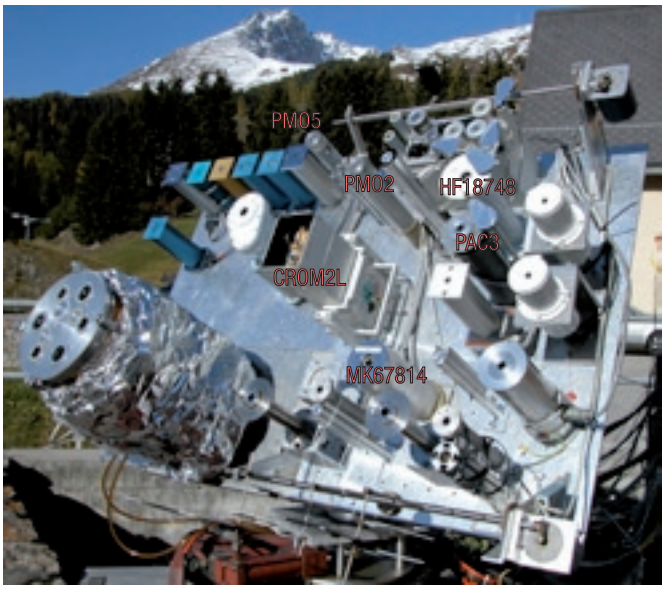

Figure 2. The World Standard Group of pyrheliometers (WSG) on the solar tracking platform. In the course of the year 2009 the three instruments HF18748, PAC3, and MK67814 were suffering from technical problems, rendering them at least temporally unavailable. PAC3 and HF18748 are operational again.

Infrared Radiometry Section (WRC-IRS)

Julian Gröbner

The Infrared Radiometry Section of the WRC maintains and operates the World Infrared Standard Group of Pyrgeometers (WISG) which represents the world-wide reference for atmospheric longwave irradiance measurements.

Performance of the WISG

The WISG operated continuously during the whole of 2009, showing an excellent relative stability between individual instruments of ±1 Wm^{-2}. For the third consecutive year each WISG instrument was calibrated in the PMOD reference blackbody, showing no significant changes in the respective responsivity over this time span. This yearly calibration procedure is used as an independent check of the WISG long-term stability.

The Infrared Integrating Sphere Radiometer IRIS

The IRIS Radiometer has been operating since November 2008 during 53 precipitation-free nights alongside the WISG. Figure 1 shows the average nightly differences between the individual WISG pyrgeometers to the IRIS Radiometer. A systematic variability between the WISG pyrgeometers and the IRIS Radiometer is apparent, with maximal differences of -3 Wm^{-2} in October to +7 Wm^{-2} in January and February. This variability seems to be correlated to the integrated water vapour content in the atmospheric column obtained from co-located GPS measurements and points towards an effect related to the spectral transmission of the pyrgeometer domes in combination with the spectra of downwelling longwave radiation. A detailed explanation of these observed differences using radiative transfer modelling is still in progress.

A second IRIS Radiometer with smaller geometric dimensions and a windowless pyroelectric detector was developed and put into operation in October 2009. Outdoor comparisons between the two IRIS Radiometers during 14 clear nights have shown remarkably consistent results within 2 Wm^{-2} as can also be seen in Figure 1.

Outlook

The two IRIS radiometers will be deployed alongside the WISG whenever conditions are favorable. Routine measurements during 2010 are expected to confirm the results obtained with IRIS 1 during 2009 and demonstrate the traceability of atmospheric longwave irradiance to the PMOD reference blackbody via the two IRIS Radiometers which are used as transfer standards.

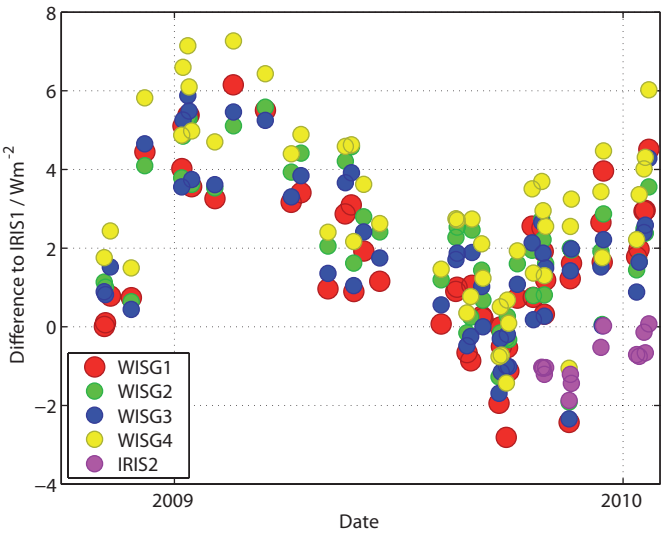

Figure 1. Night average longwave radiation from the WISG and IRIS 2 relative to IRIS 1 between 1 November 2009 and 31 January 2010. The measurements of IRIS 2 start in October 2009 and agree very well with IRIS 1.

Atmospheric Turbidity Section (WRC-WORCC)

Christoph Wehrli and Stephan Nyeki

The PFR network has grown from 12 original stations to currently 21 sites by the association of 9 European and Antarctic stations. A first Newsletter was issued to network partners and interested parties. The WORCC AOD reference was slightly adjusted after the incorporation of an instrument calibrated at Izaña on Tenerife. Four site audits were conducted for the EUSAAR project.

Three national meteorological or research institutes (FMI, Finland, SMHI, Sweden, and NILU, Norway) joined the GAW-PFR network in 2009 with 7 associate stations located in Scandinavia and Antarctica. A list of all 21 stations can be found at www.pmodwrc.ch/worcc.

After many years of reliable operation the instrument cable started to fail at Izaña and required an overhaul of the complete data logger system at Davos. Similar refurbishments were made for the stations at Alice Springs (Australia) and the Jungfraujoch (Switzerland).

Figure 1. Map showing the locations of 7 associated GAW-PFR stations in Northern Europe. Two additional stations, Marambio (FMI) and Troll (NILU) are located in Antarctica.

Due to several technical and logistical problems no data were obtained in 2009 from Mt. Waliguan (China). The PFR was severely damaged by a tracker malfunction and is currently at Davos for repair.

A passive wind-screen was shipped to Cape Point, South Africa, where it has proven to be an effective measure against window contamination by dust and sea-spray.

In 2009, seven instruments of the extended GAW-PFR network were calibrated against the reference Triad at Davos, and 5 instruments were calibrated by Langley method at their proper sites.

The primary calibration of the Izaña instrument was used upon its return to Davos to verify the stability of the WORCC calibration Triad. After careful intercomparisons, four coefficients of the 3*4 channels were adjusted by 0.5 % and one coefficient by 1 %. After incorporation of the Izaña instrument, the Triad scale shifted by 0.8 % at most. In an agreement between the Meteorological Agency of Spain and WORCC, the Izaña site was established as a primary calibration facility for the GAW-PFR network.

As of January 2010 the World Data Centre for Aerosols (WDCA) moved from JRC Ispra to NILU where it will be integrated into the EBAS data warehouse (http://ebas.nilu.no/). Data files will be converted from NARSTO to AMES format. Protocols for delivery of AOD data in NRT within the scope of WIGOS are being developed by NILU and WORCC. Previous AOD data are still available at JRC Ispra.

Two new PFRs equipped with filters at 1024, 946, 817, 778 nm and at 719, 675, 610, 450 nm were built to become reference instruments covering the extended set of WMO recommended wavelengths after their full calibration.

Four station audits and AOD inter-comparison campaigns were conducted at the EUSAAR sites Finokalia (Greece), Demokritos (Greece), at the Institute for Tropospheric Research in Leipzig (Germany), and at the GAW Izaña site.

A first Newsletter was prepared and sent to PFR users and interested parties. It is foreseen to publish additional Newsletters on an annual or semi-annual basis.

Maintenance of the PFR Calibration Triad at WORCC

Christoph Wehrli, Stephan Nyeki, and Julian Gröbner

A Triad of Precision Filter Radiometers (PFR) serves as a conventional scale for the calibration of PFRs deployed in the GAW-PFR network. This Triad is composed of PFR instruments that were Langley calibrated at high altitude stations. Their internal consistency is monitored by routine cross-calibration as described in the PMOD Annual Report 2008. At least once per year one of the Triad members is substituted by a newly calibrated instrument in order to assure the long-term stability of the WORCC reference.

The Izaña Atmospheric Research Center (IARC) situated at 2373 m a.s.l. on Tenerife Island offers excellent conditions for Langley extrapolations. It is a designated GAW global station and serves as a primary calibration site for the PHOTONS and RIMA European branches of the AERONET federated network.

The PFR instrument N25 was recalled in spring 2009 from IARC to become a member of the WORCC Triad. Results of a comparison between calibrations determined by Langley extrapolations at Izaña in December 2008 and January 2009 and by cross-calibrations against the Triad revealed a 2σ significant difference of 1.2 % in the 368 nm channels. Differences in the other channels were below 1 % and not significant at the 2σ level.

	862	500	412	368
N01	1.000	1.000	0.995	0.990
N25	1.000	1.000	1.000	1.000
N26	1.000	1.000	0.995	0.995
N27	1.000	1.000	1.000	0.995

Table 1. Correction factors applicable to individual channels of the WORCC Triad, based on Izaña Langley calibrations of the PFR instrument N25.

In a next step, the individual members of the Triad were cross-calibrated against the Langley calibrated PFR-N25. The relative change between calibration constants in use and those obtained from comparison with PFR-N25 can be attributed with equal contributions to an aging of the Triad channels and to the uncertainty of the Langley calibrations. Based on this calibration, an aging of the Triad is taken into account by correction factors (see Table 1) that have been applied since July 2009 to the calibration constants of the original Triad. As the uncertainty of calibrations and comparisons involved are of the order of 0.5 %, the correction factors are rounded to the next multiple of 0.005.

At the beginning of January 2010, the Triad instrument N26 was substituted for N25. With respect to its realization during the Filter Radiometer Comparison in 2005, the 'new' WORCC Triad has changed by -0.2 % at 412 nm and by -0.8 % at 368 nm.

PFR-N26 was subsequently installed at Jungfraujoch for calibration by Langley extrapolations. First results are excellent and confirm the adjusted Triad scale, except for the 368nm channel, where a slightly smaller correction is at present suggested.

In summer 2010, an instrument calibrated at Mauna Loa will be integrated into the WORCC Triad, and the 3rd Filter Radiometer Comparison in autumn will be an occasion to establish the relation of instruments used in global AOD networks to the WORCC reference.

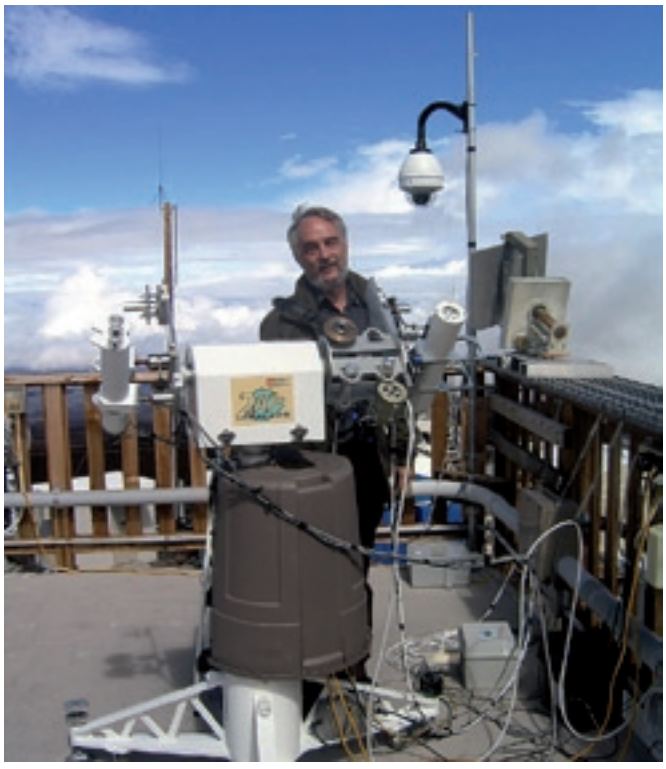

Figure 1. Christoph Wehrli visiting the PFR site Mauna Loa on December 4, 2007.

EUSAAR: Aerosol Optical Depth Inter-Comparison Campaigns

Stephan Nyeki, Christoph Wehrli, and Julian Gröbner

WORCC activities within the EU FP6 EUSAAR program continued in 2009 with AOD inter-comparison campaigns at 4 European sites. The strict WMO criterion for calibration traceability was narrowly missed by two stations.

The EUSAAR program aims to integrate and harmonize measurements of aerosol optical properties at European observation sites, amongst other goals. WORCC is participating in EUSAAR by conducting audits and aerosol optical depth (AOD) inter-comparison campaigns at sites with existing, extensive aerosol measurement programs, so-called super-sites.

In 2009, one audit at Izana (Canary Islands) and three AOD inter-comparisons at Finokalia (Crete, Greece), Athens (Greece) and Leipzig (Germany) were conducted. These sites have CIMEL sun-photometers federated to the AERONET AOD network which measured alongside a WORCC PFR (precision filter radiometer) travelling standard.

The quality of AOD data from the inter-comparison can be gauged according to WMO criteria. These state that inter-comparisons should be over a sufficient period of time to ensure that: a) N ≥ 1000 coincident AOD data points are collected, b) a minimum of 5 clear sunny days, and c) AOD at 500 nm should be in the range 0.040 - 0.200. If these conditions are met, then traceability occurs when 95 % of CIMEL-PFR points lie within limits defined by Eq. 1 where m = airmass:

$$U_{95} < \pm (0.005 + 0.010/m) \qquad \text{Eq. 1}$$

Measurements during the Athens campaign were particularly interesting and are further described. The PFR was located at two different sites: ISARS/NOA (191 m asl; CIMEL), and the GAW Regional site at the Demokritos Institute (267 m; 3 km distant from ISARS/ NOA). Figure 1a-b illustrates the CIMEL-PFR AOD difference (λ(nominal) = 865 nm) versus airmass at ISARS/ NOA and Demokritos, respectively. The WMO criterion for traceability was nearly met at ISARS/NOA with 89.4 % despite only N = 462 coincident measurements, while traceability was not met at Demokritos with 46.4 % and N = 1265. Nevertheless, the low CIMEL-PFR AOD difference (-0.012 and 0.004 at 500 and 865 nm; campaign average) at ISARS/NOA suggests that the WMO goal of AOD uncertainty <0.015 is achieved in routine AERONET operations. This was not achieved at Demokritos as the PFR and CIMEL were not co-located, in addition to a difference in altitude. This case illustrates the well-known observation that aerosol concentrations are in general only homogeneous over short horizontal or vertical extents. AOD and in-situ aerosol measurements that are too distant apart, as is the case at several EUSAAR super-sites, may therefore be difficult to interprete.

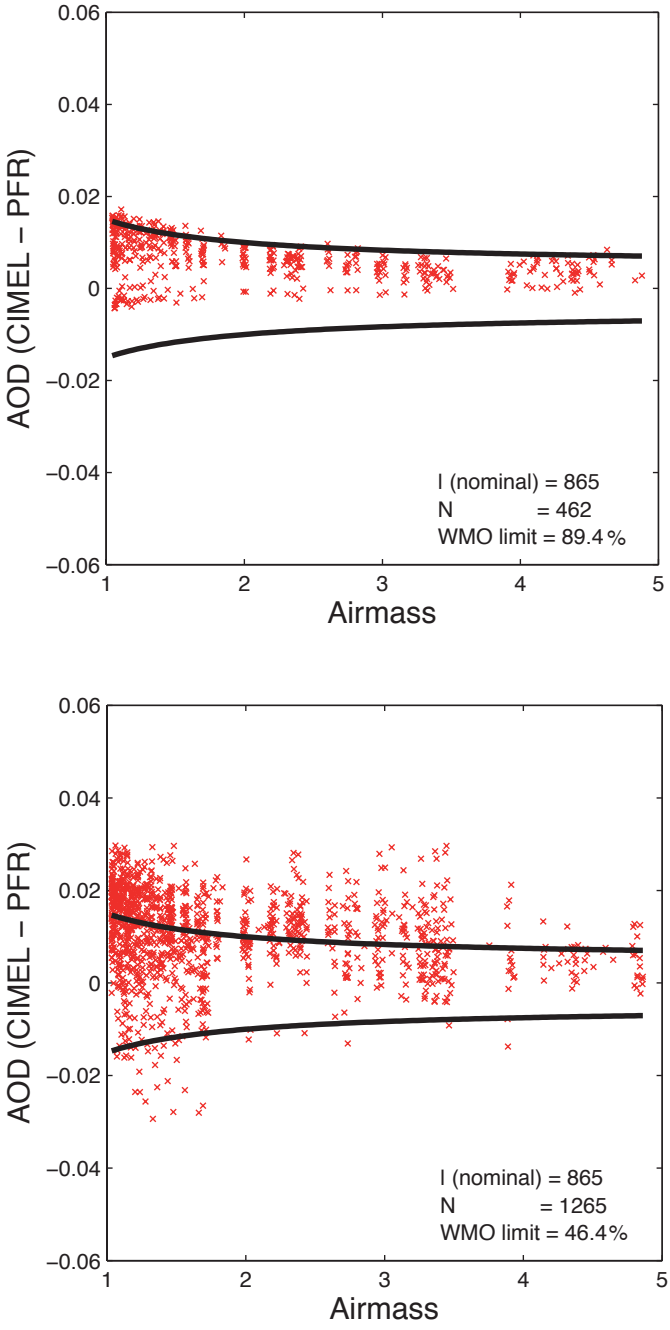

Figure 1. CIMEL-PFR AOD difference (λ = 865 nm) versus airmass, illustrating the WMO criteria for traceability (solid line) at: ISARS/NOA (upper panel), and Demokritos (lower panel).

Further on-site audits and AOD inter-comparisons will be conducted at the Birkenes (Norway) and Puy de Dome (France) EUSAAR-sites in 2010.

European Ultraviolet Calibration Center (EUVC)

Julian Gröbner and Gregor Hülsen

The Global Atmospheric Watch (GAW) Ultraviolet (UV) Calibration Center aims at improving the data quality in the European GAW UV network and at harmonizing the results from different stations and monitoring programs in order to ensure representative and consistent UV radiation data on a European scale.

In July the UV radiometers located at PMOD/WRC and at the Messfeld-Weissfluhjoch were calibrated relative to the QASUME reference spectroradiometer. The calibration factors for 2009 for all instruments varied by ±2 % or less relative to the previous calibration performed in 2008.

An extensive quality control of the UV data obtained since late 2006 at PMOD/WRC was undertaken in 2009; a quality assured data set was obtained by homogenising the time series and combining the measurements from the different instruments.

Quality assurance audits with the transportable reference spectroradiometer QASUME were performed at four sites: The Quality Assurance in the Arctic (QAARC) field campaign at Ny-Ålesund, Spitzbergen, Norway, in May, the Agencia Regionale per la Protezione del' Ambiente (ARPA) in Valle de Aosta, Italy, in August, the Agencia Estatal de Meteorologia (AEMET), in Madrid, Spain, in September, and the Regional Brewer Calibration Center Europe (RBCC-E) campaign at El Arenosillo, Spain, also in September.

The highlight of 2009 was clearly the inter-comparison of two spectroradiometers and four UV filter radiometers at Ny-Ålesund, Spitzbergen, Norway, with our reference spectroradiometer QASUME. Scientists from Germany, Norway and Italy participated at this intercomparison which was partly funded by the European Center for Arctic Environmental Research (ARCFAC). This first intercomparison of UV spectroradiometers at such a high latitudinal site has demonstrated that solar UV measurements can be performed reliably in the harsh Arctic environment.

Results of all the QASUME site audits can be found at the EUVC web-site:

http://www.pmodwrc.ch/euvc/euvc.php?topic=qasume_audit

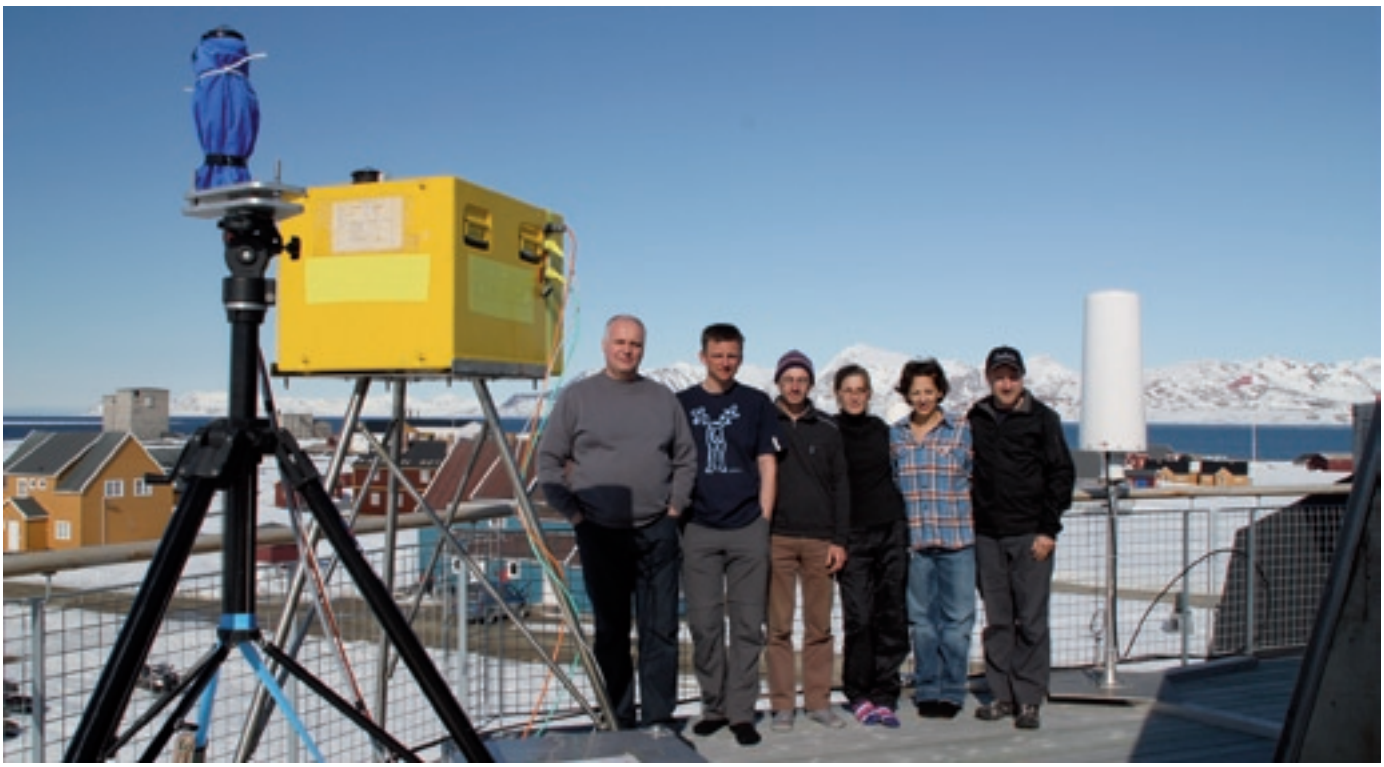

Figure 1: Group photo of the participants at the intercomparison of solar UV spectroradiometers and multifilter radiometers at Ny-Ålesund, Svalbard, Norway.

Instrument Development

Instrument Sales

Silvio Koller

In 2009, four Precision Filter Radiometers (2 Germany, 1 Japan, 1 WORCC) and three Absolute Radiometers (1 Mexico, 1 Hong Kong, 1 Lithuania) were sold. As a consequence, the number of in-stock instruments has decreased significantly, and the manufacture of new series has to be envisaged.

Figure 1. Precision Filter Radiometer N049 of MetEire in Valentia, Ireland.

Solar Radiometry Section

Wolfgang Finsterle

The Solar Radiometry Section is currently engaged in three development projects for new radiometers. The digitally controlled radiometer with phase-sensitive signal analysis is planned as a successor of the current PMO6 type for ground-based measurements as well as for space applications. The Monitor for Integrated Transmittance (MITRA) is part of the Cryogenic Solar Absolute Radiometer (CSAR) project to better integrate solar radiometry in the SI international system of units. The terahertz absolute radiometer will be the first absolute standard for terahertz radiation worldwide. It is thought to provide the metrological basis for this emerging field of radiation technology.

The Cryogenic Solar Absolut Radiometer (CSAR) and the Monitor for Integrated Transmittance (MITRA)

PMOD/WRC developed and built the Monitor for Integrated Transmittance measurements. MITRA is a core part of the Cryogenic Solar Absolute Radiometer (CSAR). Based on the tests with the first MITRA prototype (see annual report 2008) an improved thermal and mechanical design was developed and built (Figure 2). Thermal stability testing confirmed that the new design will allow the integrated transmittance of a window within the required uncertainty levels of better than 1 part in 105 (100 parts per million, see Figure 1) to be measured.

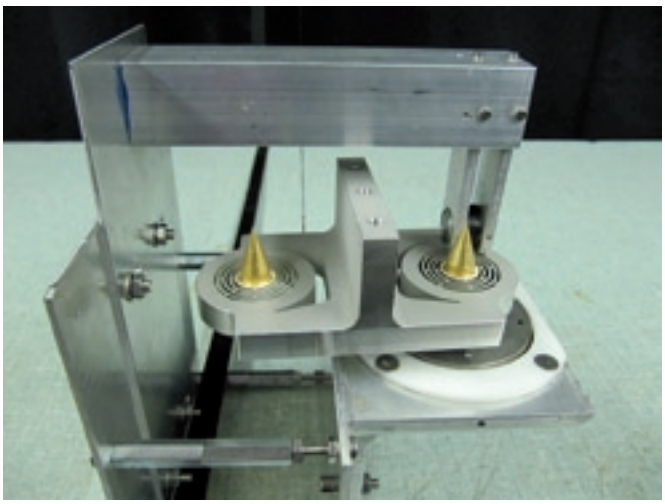

Figure 1. The MITRA cavit/heatsink assembly sits on the rotating table, waiting to be equipped with copper-wire thermometers.

Laboratory testing will be finished by April 2010, when MITRA will be installed on the solar tracking platform to prove its capabilities under real-world conditions. Meanwhile all parts for the cryogenic section of the CSAR have been designed by the National Physical Laboratory (NPL) in Teddington, UK, and manufactured by METAS and the private Swiss sub-contractor Innotool. André Fehlmann of PMOD will assist with the final assembly of the CSAR at NPL in spring 2010 before the CSAR will be brought to PMOD for integration on our solar tracking platform.

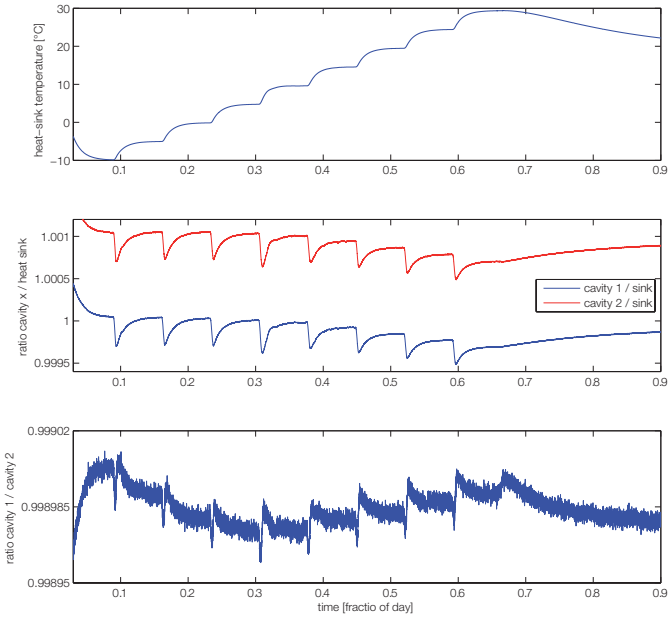

Figure 2. Results from the thermal stability test performed in the climate chamber. The top panel shows the temperature of the heat sink. The bottom panel is the ratio of the temperature enhancement in both MITRA cavities. During nominal operation a window will be placed in front of one of the cavities, the ratio is then equal to the integrated transmittance of the window. As can be seen in the lower panel the ratio is extremely stable, varying less than +/-30 parts per million over the temperature range from -10 to +30 °C.

Digitally controlled radiometer with phase-sensitive signal analysis

A new digital control unit for absolute radiometers was built and tested in 2009. This control unit allows the radiometer to be operated with a much faster shutter cycle (~20 seconds instead of 180 seconds with the analog control loop), an important prerequisite for the phase-sensitive processing of the solar irradiance signal. The PMOD/WRC internal publication //corona/pmod/instruments/PMO-PhaseSensitive/DigitalRadiometer/Documentation/Documentation_DRM.doc (need to assign a publication number).

The absolute radiometer for Terahertz (THz) radiation

During summer of 2009 the Physikalisch Technische Bundesanstalt (PTB) in Berlin and the PMOD/WRC investigated the design of a THz absolute radiometer based on the principle of electrical substitution in a feasibility study. We quickly realized that the expertise of both institutes complemented each other nicely and decided to start a formal collaboration on this problem. By November 2009 a modified PMO6-type radiometer had already been delivered to PTB Berlin to be tested on the quantum cascade laser THz source (Figure 3). The modification consisted of adapting the field-of-view geometry to the long-wavelength (0.3 to 1 mm) THz radiation and a modified shutter front surface to suppress interference with the quantum cascade laser. The test results were already very promising with the absolute uncertainty estimated to be of order of only 10 %. Characterization experiments are now under way at both institutes in order to minimize the absolute uncertainty.

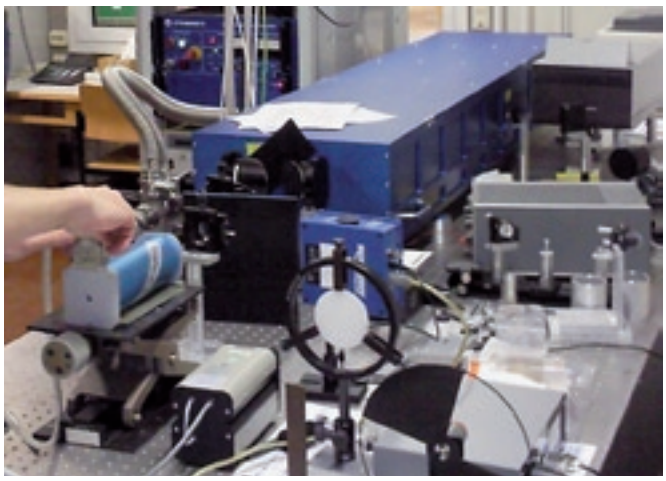

Figure 3. The modified PMO6 radiometer is being installed on the THz laser system at PTB Berlin. These test measurements yielded very promising results. The major sources of uncertainty were identified to be the absorptance of the cavity and the non-equivalence of electrical and radiative heating. The former will be measured by PTB, the latter will be determined at PMOD/WRC.

A Finite Element Model for the Investigation of Thermal Properties of a PMO6 Type Radiometer

Uwe Schlifkowitz

A finite element model has been developed to investigate the thermal properties of a PMO6 radiometer for total solar irradiance measurement. A special focus has been put on the new techniques included in the prototype instrument, the so-called phase-sensitive signal detection and the digital heater control. The model can successfully reproduce the effect of non-equivalence of radiative and electrical heating, which is one of the largest contribution to the absolute uncertainty of the PMO6-type radiometer. The model can easily be adapted to investigate other instruments.

The model accepts 3D CAD drawings as input. To reduce computing time, the model has been developed in 2D. The reduction from 3D included a de-featuring of the non-axisymmetric components of the geometry and a thorough comparisons to prove its validity. The geometry had to be slightly modified to account for the changes in thermal mass and thermal resistance in the specific components.

Variable solar input and changes in ambient temperature can be simulated. Therefore, it is now possible to theoretically investigate and eliminate many sources of irritation before building or modifying a prototype instrument.

Furthermore, the shutter cycle in the model can be adjusted to maximize TSI signal with regard to phase-sensitive detection, as discussed in PMOD/WRC annual reports 2007 and 2008.

Currently, the model is capable of running simulations without heat loss, with heat loss by convection or radiation or a combination of these two, as shown in Figures 1 and 2. Additionally, heat loss by means of conduction through air is available. However, the combination of conduction and radiation heat loss has not yet been verified.

With the help of this model, it is possible to investigate heat losses and thermal flows anywhere in the cavity. Important issues

such as the non-equivalence of the electric and radiative heating can be addressed. Furthermore, developed theories can be verified and used as a starting point for a sound characterization of the prototype instrument. Finally, the validity of the prototype data obtained from measurements both in the laboratory and in front of the sun can be examined.

In Figures 1 and 2, results from different simulations are shown. The simulations are set up with a constant ambient temperature of T_0 = 300K and a constant solar input of TSI = 1000 W/m^2. For the simulations with radiation, an emissivity of ε=0.028 was assumed for the surfaces taken into account. Heat loss through air was estimated by free convection with a film coefficient h = 10 W/m^{2}K. An ideal thermal connection between the individual components is assumed.

After a warm-up phase of 10s the shutter with a cycle length of T = 30s starts with an open phase. The PID control loop works as expected. The strong oscillations especially at the beginning could be overcome by adjusting the PID parameters. Figure 1 shows that the temperature elevation of the cylindrical walls in irradiated state with respect to the shaded state is much larger in vacuum (difference between grey and red solid lines) than in air (difference between blue and green solid lines). Since radiative heating of the cylindrical walls is equal in both situations the difference must be caused by the much more efficient air cooling compared to the radiative cooling in vacuum. Assuming that radiative losses are negligible, the air-vacuum difference in the elevation of the temperature of the cylindrical wall is a measure for the non-equivalence of radiative and electrical heating. Although the magnitudes of the heater power (Figure 2) are significantly different for different simulation set-ups, both the difference between heater power for open and closed shutter state and the shape of the oscillations caused by the PID control loop are not. Unfortunately, the simulations are far too short for a phase-sensitive analysis. Longer simulation times and verifications of the simulation models are therefore of utmost importance.

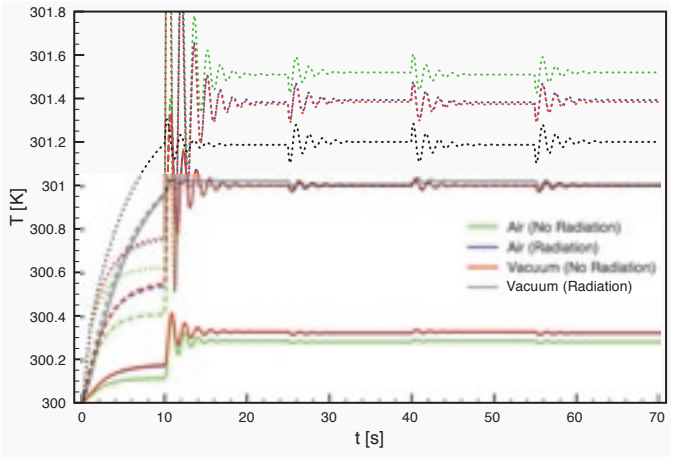

Figure 1. Simulated temperature vs. time at different locations inside the cavity. Simulations were run for three different configurations. These are a) Air without radiation (green), b) Air with radiation (blue), c) Vacuum with radiation. The dotted lines represent temperature on the cone next to the heater foil. The dashed lines represent the average temperature over the upper thermal resistor. The solid lines show the temperatures at the upper end of the cylinder.

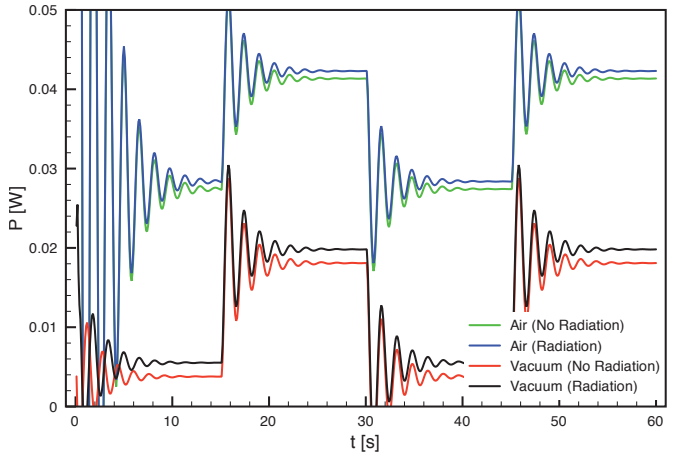

Figure 2. Heater power corresponding to the simulations shown in Figure 1. The amount of heater power is directly coupled to the heat loss, resulting in a non-equivalence of the radiative and electrical heating.

Space Experiments

Silvio Koller and Dany Pfiffner

LYRA – Lyman Alpha Radiometer

After various shifts of the launch date, PROBA-2 was finally sent into Space in November 2009, launching from the Russian cosmodrome Plesetsk. Since the LYRA Flight model was delivered to Verhaert Space, Belgium and integrated on the spacecraft more than two years ago, PMOD/WRC has had little involvement in pre-launch activities in 2009. A last cover-locking procedure was performed at prime contractor premises in May 2009, in order to prepare LYRA for the upcoming launch.

On November 2nd, 2009 the spacecraft PROBA-2 was launched together with the ESA satellite SMOS. Launch and early orbit operations of PROBA-2 were very successful. After a short outgassing phase LYRA was switched-on in space for the first time on November 16th, 2009. No science data was acquired at that time but the instrument status and housekeeping parameters showed that everything ran nominally and LYRA was ready to go operational. It is planned to perform “First light” measurements, in other words opening of the LYRA cover mechanisms, in early January 2010. The three UV filter radiometers will detect wavelength ranges in the VUV up to the Herzberg Continuum. The first two months will consist of the commissioning phase, followed by the fully operational phase. Experience from the commissioning phase will provide information concerning instrument degradation, which is to be expected. Depending on these results the backup strategy of the three instruments can be determined.

Figure 1. PROBA-2 at Verhaert Space, being prepared for shipment.

DARA

Davos Radiometer (DARA) is a newly initiated short term PRODEX project, to bridge PHASE B of the delayed PROBA-3 ESA project. DARA is intended to be the successor of our PMO-6 type space radiometers. DARA contains a complete revised cavity and also a totally new designed electronic.

This short term project lasts for one year from April 2009 to April 2010. DARA was initiated due to several reasons. The most important is that we need a prototype to learn about for future space instruments with the new cavity and electronics design. The software development for the internal microcontroller is subcontracted to a small swiss company named dlab.

At the end of the year the mechanic and cavity design was finished, see Illustration 1. The electronics definition was also completed but not all of the boards are lay-outed and assembled.

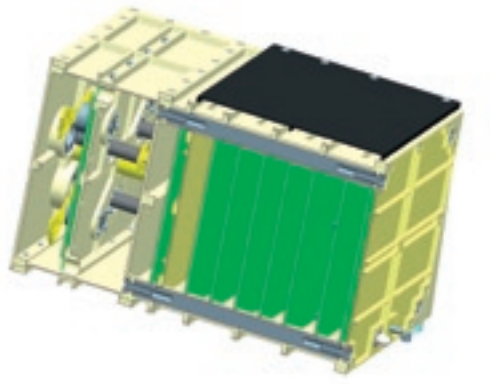

Figure 2. Cut view of DARA.

SuMo – Sun Monitor

For PROBA-3, the third mission of the ESA PROBA series, PMOD/WRC submitted a proposal at the end of 2009 for a new space experiment. It is proposed that SuMo will contain two instruments: a) a new type of absolute radiometer, based on the DARA design and b) a Sun pointing sensor, similar to the earlier TASS instruments.

PREMOS

PREMOS is a medium size space instrument aboard the French micro satellite PICARD. PREMOS is equipped with three filter radiometers, measuring three visible and three UV wavelength ranges and two PMO-6 type absolute radiometers. PREMOS was delivered for integration to CNES in summer 2009. The launch of PICARD is expected in June 2010.

During the System Level Thermal Balance Test at Intespace in Toulouse we detected that one of the two PMO6 Absolute Radiometers were malfunctioning. Further investigations based on data analysis revealed that one of the cavity heater foils was broken. During the same test one of the paraffin actuators, which holds the cover in place during launch, was damaged.

Hence PREMOS was returned to our Institute to replace the Radiometer and the actuator.

This retrofit took place in August during which a further UV calibration measurement of all Precision Filter Radiometer Heads was completed. Due to perfect weather conditions it was also possible to conduct sun measurements on our tracker next to the WSG. Before the second delivery of PREMOS to CNES in mid-September could occur, an attenuated vibration test at the University of Bern was necessary.

Later in December we attended the flight readiness meeting at CNES in Toulouse. This meeting was also a success for PREMOS.

PREMOS Radiometer Calibrations

The damage of the absolute Radiometer during the thermal balance test was also a chance to perform further calibrations with the spare Radiometer before replacement.

PREMOS 0307 Absolute Radiometer

During July, André Fehlmann was in Boulder USA at the Total Solar Irradiance Facility (TRF). During three weeks at the TRF he conducted a power and irradiance comparison with the PREMOS spare Radiometer against the cryogenic radiometer in vacuum. He also performed so-called non-equivalence measurements at this facility.

PREMOS 0107 Absolute Radiometer

This Radiometer exhibited abnormal behavior during the system level thermal balance test. Investigations showed that the front heater resistor has become unstable. However, it is still possible to correct irradiance measurements.

This instrument was in Boulder after replacement in October.

André Fehlmann conducted the same measurements at TRF as with the spare instrument. Additional stray light measurements were carried out and he also performed aperture heating simulations.

For more information about this measurement campaign please see the Science part of this annual report.

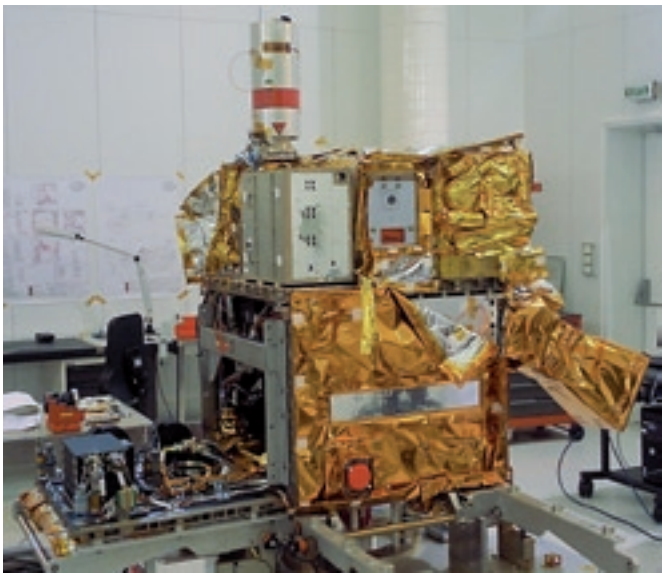

Figure 3. PREMOS integrated on PICARD beside SOVAP and SODISM.

Scientific Research Activities

Overview

Werner Schmutz

The main topics of research at PMOD/WRC are Space Climate and Space Weather. The first is the long term forcing of solar variability on the terrestrial climate, while space weather is the short term influence of outer space. In most of our projects there is emphasis on the effects of solar radiation. We address questions concerning the radiation energy budget in the terrestrial atmosphere as well as those of solar physics in understanding the mechanisms of solar irradiance variability. Hardware projects at our institute are part of investigations into Sun-Earth interactions by providing measurements of the solar irradiance.

Besides the relevance to the main research themes, there is another important aspect that governs the choice of projects to be conducted at the institute: Namely the synergy between the know-how obtained from the operational services of the World Radiation Center and other research activities. Basically, the same instruments are built for space based experiments as are utilized for ground based measurements.
The research activities can be grouped into three themes:

- Climate modeling
- Terrestrial radiation balance
- Solar physics

Basically all of the research projects are financed through third-party funding. Last year, we were supported by the Swiss National Science Foundation (5 projects), MeteoSwiss (1 project), the European Framework Program FP6 (1 project), and by a collaborative project within the first space science research call of the seventh Framework Program FP7 (1 project). The hardware development of space experiments is paid by the ESA PRODEX program (3 projects). These funding sources supported 6 PhD Theses, 3 post docs, and 4 engineers and technicians.

The PMOD/WRC contribution to the SOTERIA FP7 project is on the one hand the irradiance measurements of its LYRA and PREMOS space experiments. The observational data will be available on-line in near-real time to the space weather community. On the other hand, we intend to publish on the internet an operational “nowcasting” of the chemical composition of the middle atmosphere. Photochemical reactions under the influence of the variable UV irradiance as observed by the space experiments will be calculated. The modeling tool is a 3-D coupled Chemistry-Ionosphere-Climate model, SOCOLI[i], which has been developed at PMOD/WRC. For the preparation of the nowcast we have performed a sensitivity study of model simulations to assess the expected reliability of the resulting chemical composition.

The climate group has simulated 140 years from the year 1960 to 2100, based on predicted future climate scenarios. The aim was to evaluate the recovery time of ozone concentrations with respect to the mean value for the 1978 to 1983 period. Due to increased greenhouse gas concentrations the recovery will be much faster than could be expected without this influence and the ozone concentration can be expected to have recovered by 2020 in the northern hemisphere. By the end of the 21st century the predicted state of ozone concentrations will be a depletion over the tropics and an increase at latitudes larger than 30° in both hemispheres. The results will be used for the next WMO ozone depletion assessment.

Theoretically, there is a direct relation between an increase of atmospheric infrared radiation and the surface temperature. An analysis of observational measurements by the Alpine Surface Radiation Budget network from 1995 to 2008 confirmed that there is a positive overall trend. Interestingly, if the trends are analyzed for individual months then it is found that the trends are only positive for April to October whereas for December to March there is a negative trend. However, a statistical test showed that the results are not yet significant at a 95 % level.

The solar group has improved the solar atmosphere code COSI by incorporating molecular lines. The improved version agrees excellently with the spectrum of the quiet Sun as observed by SOLSTICE and SIM on the SORCE satellite. It is demonstrated that to in order to obtain agreement with the observations it is important to account for the effects of non-local thermodynamic equilibrium. As preparation for the upcoming PICARD mission, the COSI code is being used to predict the shape of the solar limb. One of the main goals of the PICARD mission is to measure the solar diameter with unprecedented accuracy, and to follow the predicted variation of the solar diameter over a solar activity cycle.

Total Ozone Recovery and its Sensitivity to Different Forcing Factors

Eugene Rozanov, Tatiana Egorova and Werner Schmutz in collaboration with IAC ETH, Zurich and MGO, S. Petersburg, Russia

With CCM SOCOL v2.0 we have simulated the evolution of the climate, chemistry and ozone from 1960 up to 2100 using several combinations of forcing factors. The simulated time of the total ozone recovery from anthropogenic halogens varies from 2005 to 2035 depending on the latitude and season. Emission of greenhouse gases greatly accelerates the recovery.

We have carried out a 3-member 140-year long transient ensemble simulation with CCM SOCOL (Schraner et al., 2008) spanning the second half of the 20th and entire 21st centuries driven by the prescribed time evolution of the sea surface temperature (SST), sea ice distribution (SI), greenhouse gases (GHG), ozone depleting substances (ODS), and sources of CO and NO_x. In addition to this reference run (REF) we performed two sensitivity simulations with fixed 1960 monthly mean GHG (NoGHG) and SST/SI (NoSST) values, and one simulation where two powerful volcanic eruptions were introduced in March 2032 and June 2041 (VOLC).

Figure 1 illustrates the recovery time of the total ozone obtained from the experiment REF. The recovery time is defined as the year after 2000 when the total ozone reaches its pre-"ozone hole" value in 1978-1983.

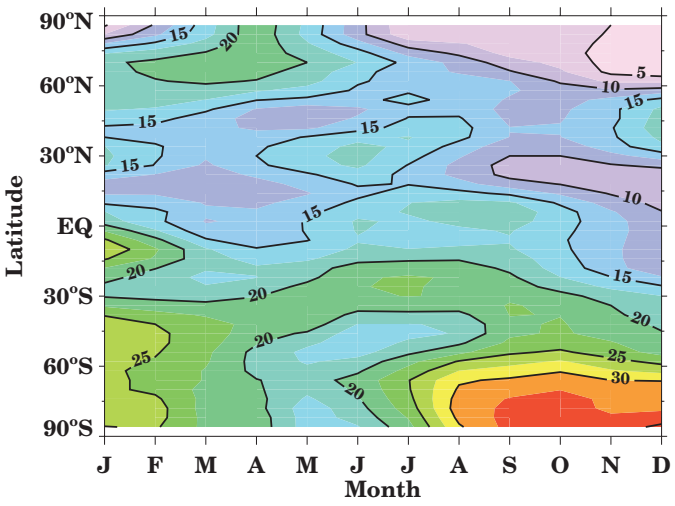

Figure 1. Recovery time (years after the year 2000) of monthly mean total ozone simulated in the REF experiment.

The recovery time varies from 2005 in the fall over the Northern hemisphere to 2035 in the Southern hemisphere during austral spring and early summer. The total ozone recovery occurs well before the recovery of the stratospheric halogen loading caused by the anthropogenic emission of organic chlorine and bromine containing substances, which is expected to happen between 2030 and 2070. The acceleration of the total ozone recovery relative to stratospheric halogen loading recovery is caused by stratospheric cooling, tropospheric/surface warming and subsequent circulation changes due to a prescribed increase of man-made GHG atmospheric abundances. It is also of interest to estimate the influence of powerful volcanic eruptions which could take place in the future, because they can influence the total ozone and climate, albeit during rather short (2-3 years) period of time.

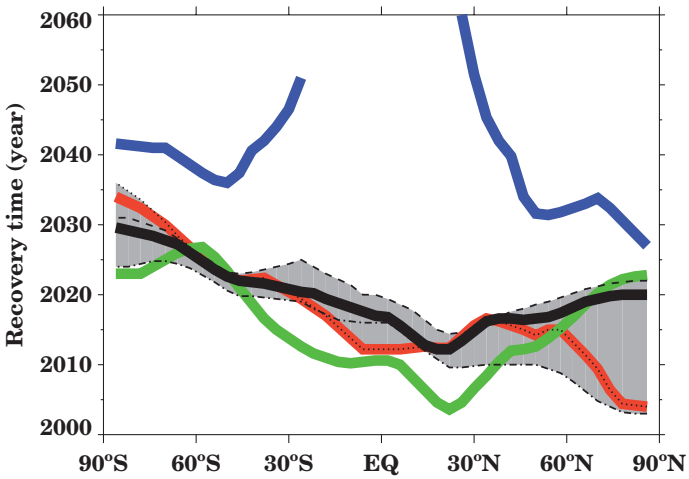

Figure 2. Latitudinal distribution of the annual mean total ozone recovery time for the experiments: REF (black lines), NoGHG (blue line) NoSST (green line), VOLC (red line). Solid black line represents ensemble mean. Thin back lines represent individual members and the shaded area shows the scatter of the ensemble.

To elucidate the role of different forcing mechanisms we analyze the output of our sensitivity runs. Figure 2 illustrates the recovery time of annual mean total ozone obtained from all sensitivity simulations. In the absence of an increase in GHG the recovery of the total ozone (blue line) is delayed by 10-40 years in the extra-tropics. In this case the tropical total ozone has not even recovered in 2100. Changes in the state of the oceans slightly (by ~10 year) decelerate the recovery process, mostly in the tropical atmosphere. The influence of the two powerful volcanic eruptions (red line) does not have substantial implications for the total ozone recovery.

The obtained results were made available for the science community via the British Data Center and will be used for the WMO Ozone depletion assessment.

References: Schraner M., Rozanov E., Schnadt Poberaj C., Kenzelmann P., Fischer A., Zubov V., Luo B., Hoyle C., Egorova T., Fueglistaler S., Brönnimann S., Schmutz W., Peter T.: Technical Note: Chemistry-climate model SOCOL: version2.0 with improved transport and chemistry/micro-physics schemes, Atmos. Chem. Phys., 8, 5957-5974, 2008.

Changes of the Ozone Layer during the 21st Century

Eugene Rozanov, Tatiana Egorova, and Werner Schmutz in collaboration with IAC ETH, Zurich and MGO, S. Petersburg, Russia

We have simulated the evolution of the climate, chemistry and ozone from 1960 up to 2100 using several combinations of forcing factors. The deviation of the future total ozone from its pre "ozone hole" state consists of the increase in the extra-tropical atmosphere and depletion over the tropics. Changes in the ocean temperature play a major role in the tropics, the contribution from ozone depleting substances dominates over the southern high-latitudes, while all factors are almost equally important over the northern high latitudes.

We have carried out a 3-member 140-year long transient ensemble simulation with CCM SOCOL (Schraner et al., 2008) spanning the time interval 1960-2100 forced by the prescribed time evolution of the sea surface temperature (SST), sea ice distribution (SI), greenhouse gases (GHG), ozone depleting substances (ODS), and sources of CO and NO_x. In addition to this reference run (REF) we performed three sensitivity simulations with fixed 1960 monthly mean GHG (NoGHG), ODS (NoODS), and SST/SI (NoSST) values.

The future changes are defined as the difference between total ozone averaged over the years 2096-2100 and over the reference period (1978-1982). Figure 1 illustrates this difference obtained from the experiment REF.

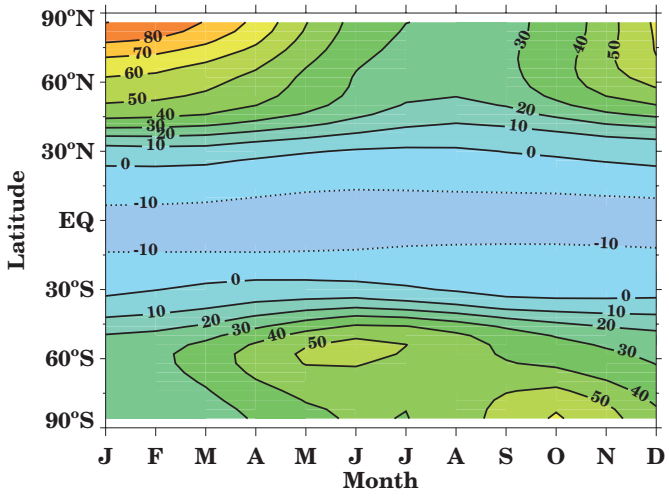

Figure 1. The difference between total ozone (D.U.) averaged over the years 2096-2100 and over the reference period (1978-1982).

The behavior of the ozone layer in the 21st century is defined mainly by the decrease of stratospheric halogen loading due to abolition of anthropogenic ODS emissions and climate change (e.g., stratospheric cooling, tropospheric/surface warming, and intensification of the meridional circulation) due to constantly growing emissions of anthropogenic GHG. While the reduction of the halogen loading and stratospheric cooling decelerate ozone destruction, more intensive meridional circulation redistributes ozone by moving it from the tropics to middle and high-latitude areas, therefore at the end of 21st century the total ozone over the tropical area decreases by ~15 D.U. and increases over the extra-tropics.

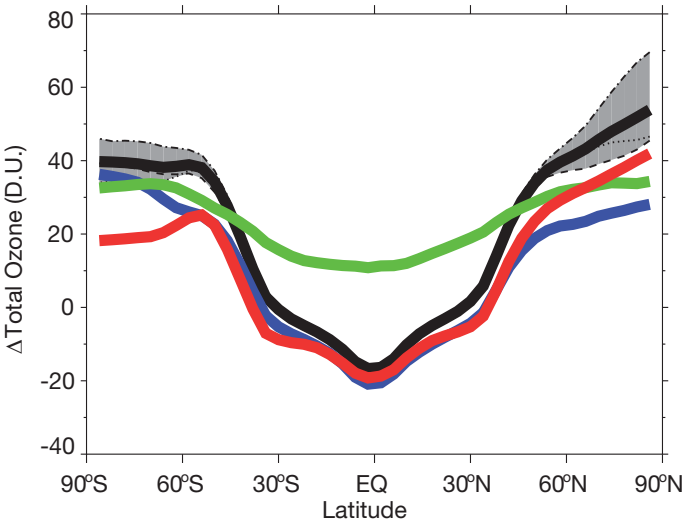

Figure 2. Latitudinal distribution of the annual mean total ozone difference between total ozone averaged over the years 2096-2100 and over the reference period (1978-1982) for the experiments: REF (black lines), NoGHG (blue line) NoSST (green line), and NoODS (red line). Solid black line represents ensemble mean. Thin back lines represent individual members and the shaded area shows the scatter of the ensemble.

To elucidate the role of different factors we analyze the output of our sensitivity runs. Figure 2 illustrates the difference between total ozone averaged over the years 2096-2100 and over the reference period (1978-1982) obtained from the reference and sensitivity simulations. The changes of the ocean temperature plays a major role in the tropics, the ODS contribution dominates over the southern high-latitudes, while ocean temperature, ODS and GHG are almost equally important over the northern high latitudes.

The obtained results were made available for the science community via the British Data Center and will be used for the next WMO Assessment on Ozone depletion.

References: Schraner M., Rozanov E., Schnadt Poberaj C., Kenzelmann P., Fischer A., Zubov V., Luo B., Hoyle C., Egorova T., Fueglistaler S., Brönnimann S., Schmutz W., Peter T.: Technical Note: Chemistry-climate model SOCOL: version2.0 with improved transport and chemistry/micro-physics schemes, Atmos. Chem. Phys., 8, 5957-5974, 2008.

Response of the Middle Atmosphere to Short-Term Solar Irradiance Variability during Different Quasi-Biennial Oscillation Phases

Anna Shapiro and Eugene Rozanov in collaboration with IAC ETH, Zurich

We applied the SOCOL chemistry-climate model to simulate the response of the middle atmosphere to the short-term variability of the solar irradiance during different QBO phases. We found that ozone sensitivity to SSI changes is different for some layers of the stratosphere.

The response of the atmosphere usually derived using cross-correlation analysis depends on the atmospheric state and internal variability. One of the principal sources of the variability in ozone, hydroxyl and other species is the quasi-biennial oscillation (QBO) that is an alternation of east and west zonal wind in the tropical stratosphere with a period of 20 to 36 months.

We applied the SOCOL chemistry-climate model (Schraner et al., 2008) to conduct a simulation of the atmosphere for the years 2000-2005 to elucidate the role of the QBO phase. Figure 1 represents a time-altitude section of the tropical average monthly mean zonal wind for 2000-2005 obtained from CCM SOCOL. This figure shows that easterlies were dominant in the stratosphere during 2000 while the period from June 2003 to May 2004 is characterized by the westerly QBO phase. We performed 1-year long ensemble runs for these two periods. The runs were driven by identical daily photolysis to eliminate the influence of solar variability. The simulated time series of hydroxyl and ozone were used for calculations of the sensitivities to the change of SSI. The results are presented in Figure 2 and 3.

The hydroxyl sensitivity to SSI changes during the solar rotation cycle are almost identical for the different QBO phases while the ozone sensitivity is slightly different for the 25 - 35 km layer. Our present understanding is that this could be the consequence of several non-linear processes that occur in the atmosphere.

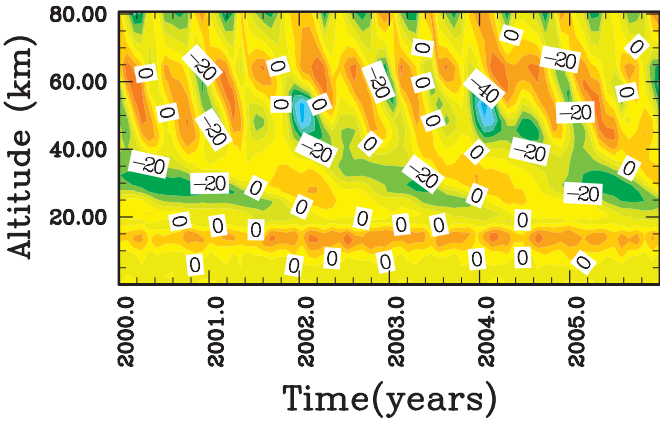

Figure 1. The tropical average monthly mean zonal wind speed in m/s for 2000-2005.

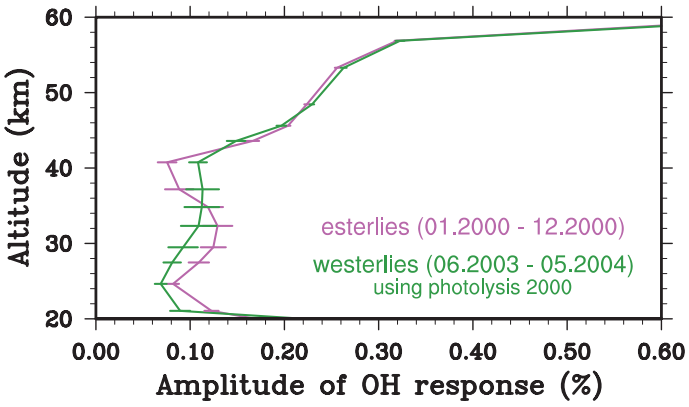

Figure 2. Hydroxyl sensitivity (in %) to SSI changes obtained in 2000 photolysis for different phases of the QBO.

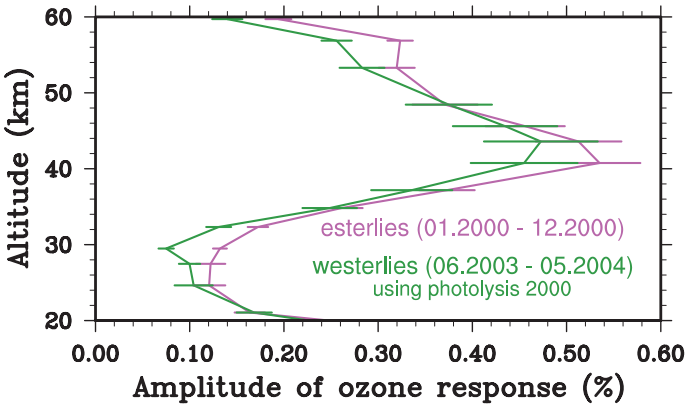

Figure 3. The ozone sensitivities (in %) to SSI change obtained with 2000 photolysis for different phases of QBO.

References: Schraner M., Rozanov E., Schnadt Poberaj C., Kenzelmann P., Fischer A.M., Zubov V., Luo B.P., Hoyle C.R., Egorova T., Fueglistaler S., Brönnimann S., Schmutz W., Peter T.: Technical Note: Chemistry-climate model SOCOL: version 2.0 with improved transport and chemistry/microphysics schemes, Atmospheric Chemistry and Physics 8, 19, 5957-5974, 2008.

Atmospheric Effects of an Extreme Solar Proton Event

Eugene Rozanov in collaboration with M. Calisto and T. Peter, IAC ETH, Zurich

We studied the influence of an extreme solar proton event (SPE) similar to the September 1859 Carrington event on atmospheric composition and temperature. Our results show that powerful SPEs have a major impact on atmospheric chemistry from the mesosphere down to the lower stratosphere, resulting in a long lasting decrease of the ozone content.

We carried out two 5-member 4-month long ensemble simulations with CCM SOCOL (Schraner et al., 2008) for August-November 1972. The control run is driven by the usual set of external forcing values. For the experiment run we applied the ionization rates used by Rodger et al. (2008) which are representative of the most extreme SPE in history (known as Carrington event) which occurred in August-September 1859.

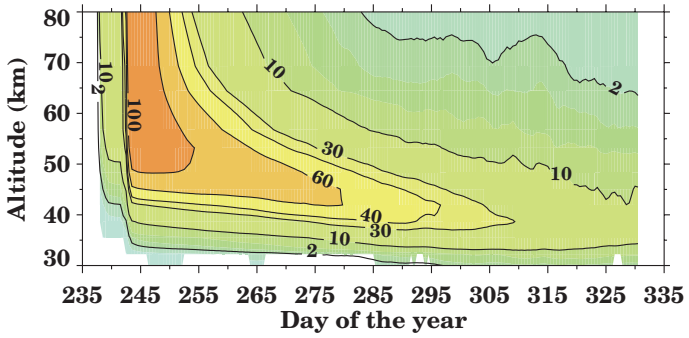

Figure 1. Simulated zonal mean NO_x changes (ppbv) over 70°N-90°N caused by the considered SPE. Color shading marks the area where statistical significance exceeds 95 %.

The ionization of the atmospheric species by solar protons results in an increase of nitrogen and hydrogen radical (HO_x and NO_x) production. Relatively short-lived HO_x leads to immediate ozone depletion, while more stable NO_x being transported down causes ozone depletion not only in the mesosphere, but also in the stratosphere. These processes are illustrated in Figures 1 and 2 which show the time-evolution of the zonal mean high-latitude NO_x and ozone changes after SPE calculated as the difference between the SPE and reference run results. The NO_x increase during SPE reaches 100 ppbv. Then, additional NO_x penetrates to the stratosphere and after ~2 month its mixing ratio still exceeds background values by ~10-20 ppbv. Substantial ozone depletion in the mesosphere during SPE is mostly caused by HO_x related catalytic cycles, but after the event ozone depletion occurs mostly in the stratosphere and is driven by NO_x. After 2 months, ozone depletion in the 30-40 km layer caused by SPE is still around 30 %. The zonal mean temperature response over northern high latitudes is presented in Figure 3.

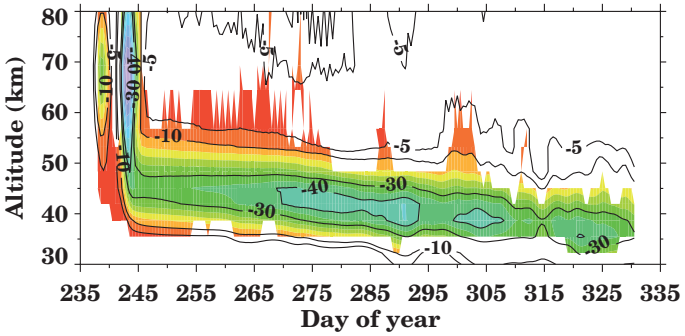

Figure 2. Simulated zonal mean ozone changes (%) over 70°N-90°N caused by the considered SPE. Color shading marks the area where statistical significance exceeds 95 %.

The cooling in the mesosphere during and just after SPE is caused by ozone depletion and a decrease of heating due to ozone absorption of solar irradiance.

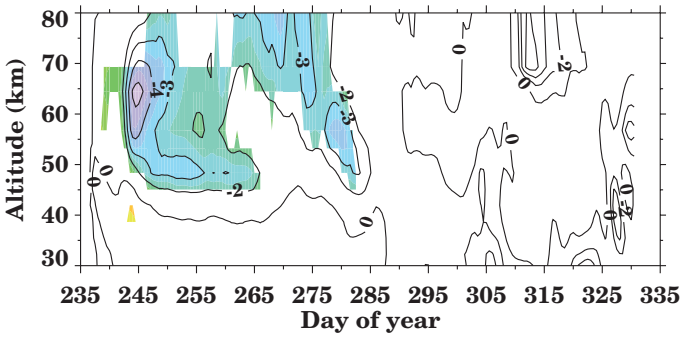

Figure 3. Simulated zonal temperature changes (K) over 70°N-90°N caused by the considered SPE. Color shading marks the area where statistical significance exceeds 95 %.

The temperature response is not observed in the stratosphere, presumably because the ozone response there appears when the solar illumination is weakened due to onset of the polar night. We do not observe any significant changes in the troposphere and near the surface, because the polar night jet is not completely formed and temperature perturbations cannot penetrate further down.

References: Rodger C.J., Verronen P.T., Clilverd M.A., Seppälä A., Turunen E.: Atmospheric impact of the Carrington event solar protons, J. Geophys. Res., 113, D23302, doi:10.1029/2008JD010702, 2008.

Schraner M., Rozanov E., Schnadt Poberaj C., Kenzelmann P., Fischer A., Zubov V., Luo B., Hoyle C., Egorova T., Fueglistaler S., Brönnimann S., Schmutz W., Peter T.: Technical Note: Chemistry-climate model SOCOL: version2.0 with improved transport and chemistry/micro-physics schemes, Atmos. Chem. Phys., 8, 5957-5974, 2008.

Modeling of the Atmospheric Response to Mt. Pinatubo Eruption

Eugene Rozanov in collaboration with IAC ETH, Zurich

We studied the influence of the Mt. Pinatubo eruption (June, 1991) on the atmosphere using simulations with CCM SOCOL and analysis of the observed data. Comparison of the observed and simulated results shows that the model overestimates the response of the tropical total ozone and stratospheric temperature.

We carried out a 3-member 46-year long transient ensemble simulation with CCM SOCOL (Schraner et al., 2008) spanning the period 1960-2006 driven by the prescribed time evolution of the sea surface temperature (SST), sea ice distribution (SI), greenhouse gases (GHG), ozone depleting substances (ODS), stratospheric sulfate aerosol (SSA), quasi-biennial oscillation (QBO), solar spectral irradiance (SSI) and sources of CO and NOx. This period of time includes three powerful volcanic eruptions. Here we concentrate on the most recent eruption (Mt. Pinatubo, June 1991) because its effects on the atmosphere were well-covered by different observation systems.

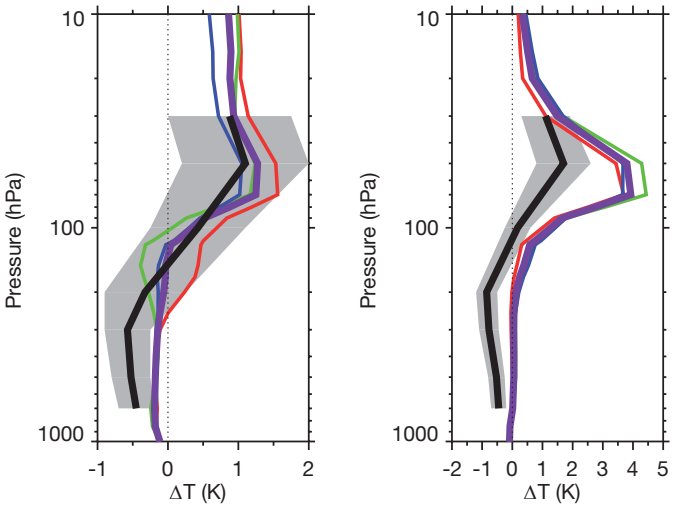

Figure 1. Global (left) and tropical (right) mean temperature response (K) to the Mt. Pinatubo eruption. The observed response is represented by the black line and the grey shading shows its uncertainty. The results of three simulations and ensemble mean are shown by red, blue, green and violet lines.

The atmospheric response as a consequence of the volcanic eruption mainly consisted of: (i) cooling of the surface and troposphere due to an increase in global albedo caused by the reflection of solar irradiance in the volcanic aerosol layer; (ii) chemical ozone depletion due to chemical processes on/in aerosol particles; (iii) warming of the tropical lower stratosphere due to aerosol absorption of infrared solar and terrestrial radiation followed by intensification of the polar night jets and suppression of the meridional circulation; (iv) ozone decrease over the extratropics and humidification of the stratosphere followed by additional ozone destruction.

To analyze the atmospheric response we follow the approach suggested by Free and Angel (2002) and compare the simulated quantities averaged over a 3-year period after and before June 1991 to diminish the influence of internal system variability and to facilitate direct comparison with observations.

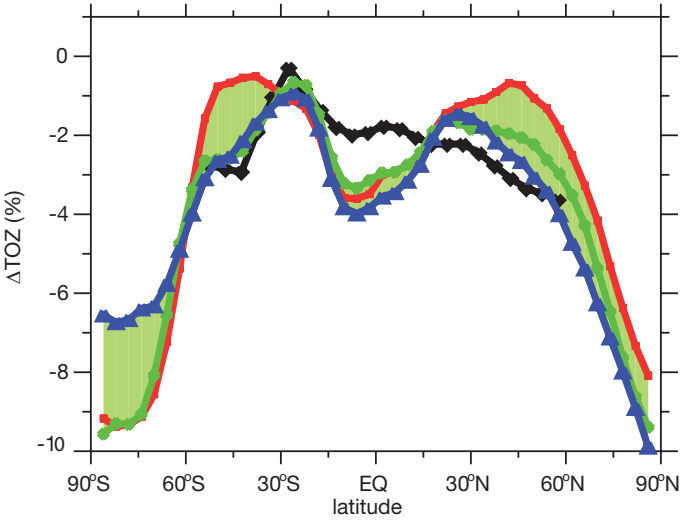

Figure 2. Total ozone response (%) to the Mt. Pinatubo eruption. The observed response is represented by the black line. The results of three simulations are shown by red, blue, and green lines. Light green shading shows the uncertainties of the simulations.

Figure 1 illustrates the simulated and observed (Free and Angel, 2002) global and tropical mean temperature response to the Mt. Pinatubo eruption. The model significantly overestimates lower stratospheric warming in the tropics and cooling over the high latitudes (not shown) which leads to reasonably good agreement of the global mean temperature response. It is interesting to note that despite the prescribed SST the tropospheric cooling is not reproduced well by the model.

Figure 2 shows the observed (obtained from TOMS measurements) and simulated responses of total ozone to the Mt. Pinatubo eruption. The model slightly overestimates ozone depletion in the tropical area. The expected strong total ozone decrease over high latitudes is difficult to validate due to poor coverage of these areas by satellite data. An analysis of the causes for the disagreement between observed and simulated data is in progress.

References:

Free M., Angell J.K.: Effect of volcanoes on the vertical temperature profile in radiosonde data. J. Geophys. Res., 107, 4101, 2002.

Schraner M., Rozanov E., Schnadt Poberaj C., Kenzelmann P., Fischer A., Zubov V., Luo B., Hoyle C., Egorova T., Fueglistaler S., Brönnimann S., Schmutz W., Peter T.: Technical Note: Chemistry-climate model SOCOL: version2.0 with improved transport and chemistry/micro-physics schemes, Atmos. Chem. Phys., 8, 5957-5974, 2008.

Climate Engineering by Injection of Sulfate Containing Gases and its Implications for the Ozone Layer

Eugene Rozanov in collaboration with P. Heckendorn and T. Peter, IAC ETH, Zurich

We simulated climate and ozone changes as a result of climate geoengineering by injection of sulfur containing gases into the stratosphere. Our results showed that this measure cools down the climate, but leads to some negative side-effects such as total ozone depletion and humidification of the stratosphere. We observe that for the future atmosphere with low halogen loading and high carbon dioxide mixing ratio the global annual mean ozone depletion may reach 3-4 % which is comparable with the ozone depletion by anthropogenic halogen emissions from 1980 to 2002.

Recently, the Royal Society published a report with the headline "Stop emitting CO_2 or geoengineering could be our only hope". This report considers a wide set of potential geoengineering measures and estimates their potential affordability, effectiveness and safety (Royal Society, 2009). It was concluded that the increase of Earth's albedo by injection of sulfate containing gases into the stratosphere is overall the most optimal way of geo-engineering, however further progress is necessary to reduce substantial uncertainty of the currently available studies and estimate possible negative side-effects. One such negative effect could be the depletion of the ozone layer caused by alteration of atmospheric chemistry and dynamics by the increased sulfate aerosol loading, a case which was observed after the Mt. Pinatubo eruption.

To estimate the potential ozone layer depletion we performed a number of 20-year steady-state experiments with CCM SOCOL v2.0 (Schraner et al., 2008) driven by the aerosol distribution and properties simulated for several geoengineering scenarios with 2-D AER aerosol model (Heckendorn et al., 2009) in off-line mode. To take into account future changes in the stratospheric composition we performed model simulations for low halogen loading, high level of CO_2, and colder sea surface which are expected in the future.

Figure 1 shows the change in annual and zonal mean total O_3 column as a function of latitude; the global mean values are listed on the plots. For the current atmosphere, the O_3 column is predicted to decrease by 4.5 % in comparison to the non-geoengineering case. This is more than the annual mean global mean total O_3 loss due to the emission of anthropogenic organic halogens, which was -3.5 % averaged from 2002 to 2005 in comparison to the 1964–1980 average as determined from observations. In the same period, observed tropical O_3 loss was negligible, while for the geoengineering scenarios, tropical O_3 loss is rather noticeable (3.5 %).

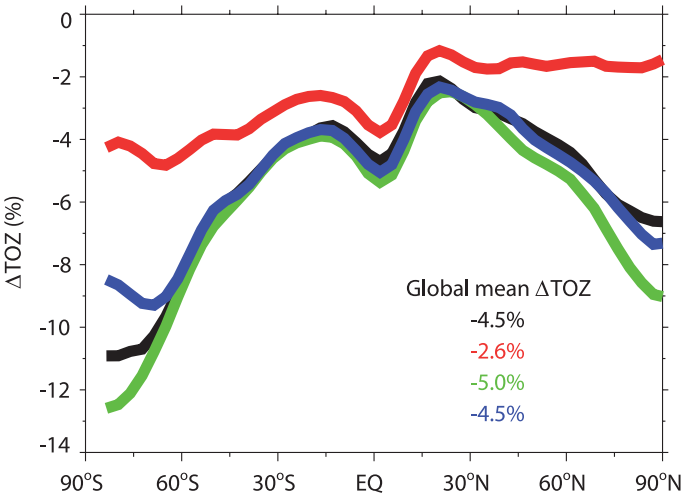

Figure 1. Change in annual zonal mean total ozone column (TOZ) due to geoengineering with continuous 5 MtS/year injections. The results have been obtained for the current atmosphere (black), low halogen loading (red), high CO_2 (green) and colder ocean surface (blue).

For the case of low stratospheric halogen loading the total ozone depletion is substantially smaller due to the smaller role of halogen related cycles. Stratospheric cooling due to CO_2 accelerates heterogeneous chemistry and leads to the enhancement of ozone depletion by sulfate aerosol, while ocean surface temperature plays a less important role. The global depletion of the ozone layer in the future due to geoengineering will therefore most likely be between 3 and 4 %.

References:

Heckendorn P., Weisenstein D., Fueglistaler S., Luo B.-P., Rozanov E., Schraner M., Thomason L., Peter T.: The impact of geoengineering aerosols on stratospheric temperature and ozone, Environ. Res. Lett., 4, doi: 10.1088/1748-9326/4/4/045108, 2009.

Royal Society Report: ‚Geoengineering the climate: science, governance and uncertainty', Royal Society Policy document 10/09, September 2009 RS1636, ISBN: 978-0-85403-773-5, London, UK, 2009.

Schraner M., Rozanov E., Schnadt Poberaj C., Kenzelmann P., Fischer A., Zubov V., Luo B., Hoyle C., Egorova T., Fueglistaler S., Brönnimann S., Schmutz W., Peter T.: Technical Note: Chemistry-climate model SOCOL: version 2.0 with improved transport and chemistry/micro-physics schemes, Atmos. Chem. Phys., 8, 5957-5974, 2008.

Simulation of the Ozone Layer without Montreal Protocol Limitations

Tatiana Egorova, Eugene Rozanov, and Werner Schmutz in collaboration with IAC ETH, Zurich and MGO, S. Petersburg, Russia

With CCM SOCOL v2.0 we simulated the evolution of the climate, chemistry and ozone from 1960 up to 2100 suggesting that the limitations on the production of the ozone destroying substances according to Montreal protocol and its Amendments were not realized.

We conducted two 140-year long transient simulations with CCM SOCOL (Schraner et al., 2008) spanning 1960-2100 driven by the prescribed time evolution of the sea surface temperature (SST), sea ice distribution (SI), greenhouse gases (GHG), ozone depleting substances (ODS), and sources of CO and NO_x. In the reference simulation (REF) we used the future time evolution of the ODS emission according to scenario A1 from (WMO, 2007). For the second simulation (noMPA) which was designed to estimate the role of the Montreal protocol limitations we applied an ODS scenario proposed by Velders et al. (2007), suggesting an ODS increase by ~3 % per year due to the absence of the limitation introduced by the Montreal protocol and its Amendments.

Figure 1 illustrates the time evolution of the global and annual mean total ozone from 1960 to 2100 for the REF and noMPA experiments as well their relative difference which can be considered as the total ozone saved by Montreal protocol implementation.

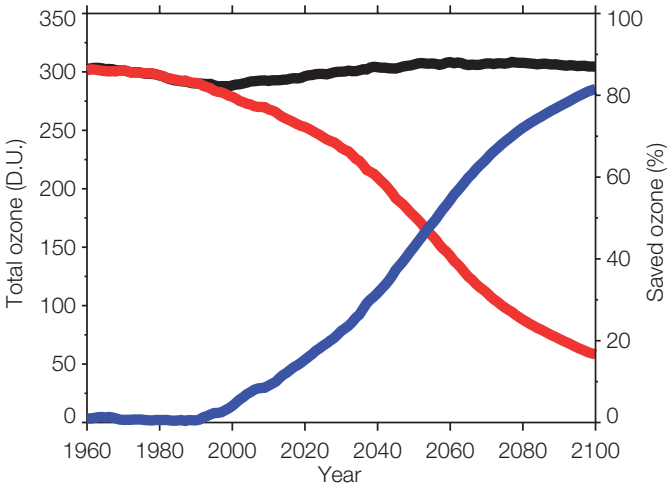

Figure 1. Time evolution of the global and annual mean total ozone for the reference (black) and no Montreal protocol (red) simulations. Total ozone saved by the Montreal protocol limitations (%) is represented by the blue line.

Figure 1 shows that the ozone destruction by increased stratospheric halogen loading is essential even for the global and annual mean ozone. The unlimited increase of stratospheric halogens leads to almost complete (~80 %) global ozone loss at the end of 21st century.

The global total ozone loss calculated as the difference between noMPA and REF results is already rather dramatic in 2030 reaching ~80 D.U. The geographical distribution of the annual mean total ozone loss for this particular year is illustrated in Figure 2.

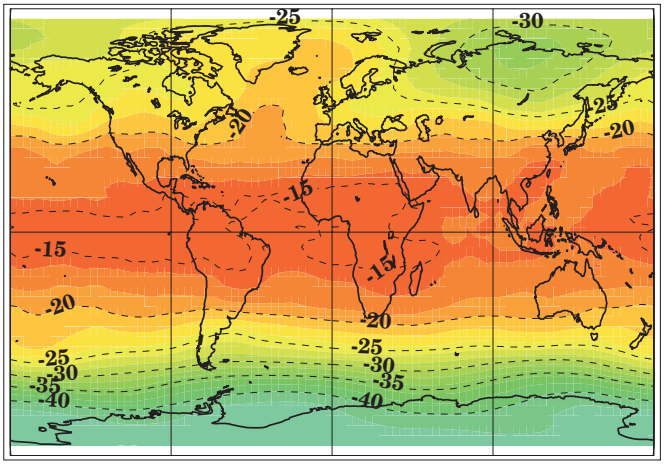

Figure 2. The geographical distribution of the annual mean total ozone loss (%) calculated as the relative deviation of noMPA from REF results for the year 2030.

As expected the most pronounced (30-40 %) total ozone loss occurs over the cold polar areas, however, even in the tropics the ozone loss can exceed 15 %. Over Europe and North America the total ozone loss is about 20 %, which could lead to an increase of dangerous erythemal irradiance by ~20-30 %. The obtained results are in general agreement with the total ozone loss estimates published by Newman et al. (2009).

References:

Schraner M., Rozanov E., Schnadt Poberaj C., Kenzelmann P., Fischer A., Zubov V., Luo B., Hoyle C., Egorova T., Fueglistaler S., Brönnimann S., Schmutz W., Peter T.: Technical Note: Chemistry-climate model SOCOL: version 2.0 with improved transport and chemistry/micro-physics schemes, Atmos. Chem. Phys., 8, 5957-5974, 2008.

Velders G.J.M., Andersen S.O., Daniel J.S., Fahey D.W., and McFarland M.: The importance of the Montreal Protocol in protecting climate, Proc. Natl. Acad. Sci. USA, 104(12), 4814–4819, 2007.

World Meteorological Organization (WMO) (2007), Scientific 971 Assessment of Ozone Depletion: 2006, Report No. 50, 572pp, Geneva, Switzerland.

Newman P.A., Oman L.D., Douglass A.R., Fleming E.L., Frith S.M., Hurwitz M.M., Kawa S.R., Jackman C.H., Krotkov N.A., Nash E.R., Nielsen J.E., Pawson S., Stolarski R.S., Velders G.J.M.: What would have happened to the ozone layer if chlorofluorocarbons (CFCs) had not been regulated?, Atmos. Chem. Phys., 9, 2113–2128, 2009.

Sensitivity of the Earth's Middle Atmosphere to Short-Term Solar Variability and its Dependence on the Choice of Solar Irradiance Data Set

Anna Shapiro, Eugene Rozanov, Alexander Shapiro, Tatiana Egorova, and Werner Schmutz in collaboration with IAC ETH, Zurich

We simulated the time evolution of neutral and charged species in the middle atmosphere using a 1-D radiative-convective model with interactive photochemistry driven by four different sets of daily Spectral Solar Irradiance (SSI). Our results showed that for the sensitivity analysis in the stratosphere based on the SSI at 205 nm any considered data sets can be applied. For the mesosphere, where the sensitivity strongly depends on the applied SSI data set more robust results can be obtained using the sensitivity calculations based on the Lyman-alpha SSI.

The solar rotation cycle of solar irradiance is a manifestation of the spatial inhomogeneity in the distribution of the bright/dark features on the solar surface and differential rotation of the Sun. A different life cycle of bright/dark features in combination with different dependences of their contrasts on the heliospheric angle leads to some phase lag between the variability of the solar irradiance at different wavelengths. The response of atmospheric species is wavelength dependent, and the inappropriate representation of this phase lag in the applied SSI data can therefore affect the estimated response of different species. We considered four data sets obtained from the SUSIM and SOLSTICE instruments onboard UARS and reconstructed by Lean et al. (2005), and Krivova et al. (2009). Figure 1 illustrates the correlation between SSI at all wavelengths and at 205 nm. For the reconstructed data sets the correlation coefficient is virtually equal to one for the wavelengths shorter than 260 nm, which means that SSI changes in this spectral area are absolutely synchronous. This is not the case for the satellite data, which show weaker correlation for shorter and longer wavelengths.

The sensitivities of hydroxyl and ozone to SSI changes are presented in Figures 2 for all considered data sets.

The ozone and hydroxyl sensitivities to SSI changes during a solar rotation cycle are almost identical for all applied SSI data sets in the stratosphere. In the mesosphere, the difference in correlation between SSI in the Herzberg continuum and Lyman-α line in considered SSI data sets leads to substantial scatter of the sensitivity estimates based on 205 nm. We conducted a sensitivity analysis based on the Lyman-alpha line and found that the sensitivity calculations based on the SSI in the Lyman-α line are more robust in the mesosphere.

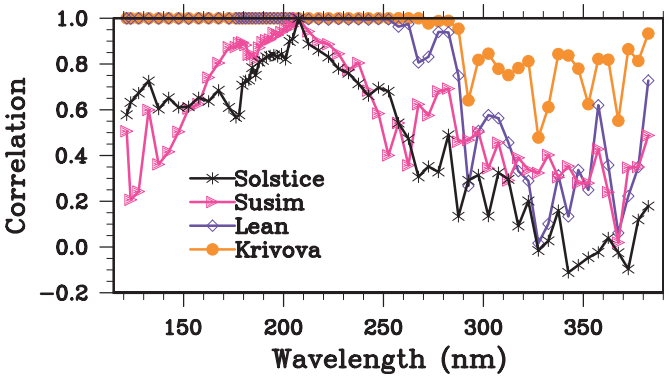

Figure 1. Correlation coefficients between daily SSI at 205 nm and all other wavelengths.

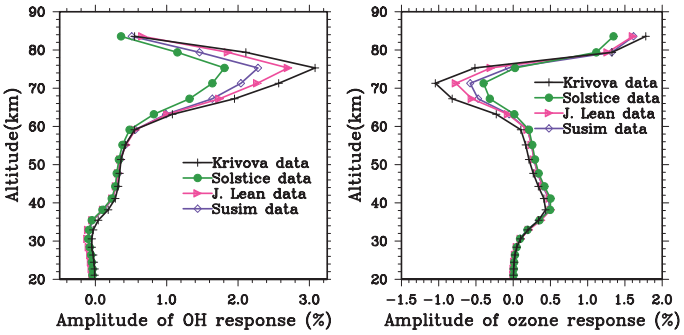

Figure 2. Hydroxyl and ozone sensitivities (in %) to a 1 % change of solar irradiance at 205 nm.

References:

Lean J., Rottman G., Harder J., Kopp G.: Sorce contributions to new understanding of global change and solar variability, Solar Physics, 230, 27-53, 2005.

Krivova N., Solanki S., Wenzler T., Podlipnik B.: Reconstruction of solar UV irradiance since 1974, Journal of Geophysical Research 114, D00I04, 2009.

Shapiro A., Rozanov E., Egorova T., Shapiro A., Schmutz W., Peter T.: Sensitivity of the Earth's middle atmosphere to short-term solar variability and its dependence on the choice of solar irradiance data set, Journal of Atmospheric and Solar-Terrestrial Physics, 2010.

Nowcast of the Middle Atmosphere and Ionosphere State with the Chemistry-Ionosphere-Climate Model SOCOL[i]

Tatiana Egorova, Eugene Rozanov, and Werner Schmutz

An important aspect of nowcast is an evaluation of the response of the middle atmosphere to the variability of the solar ultraviolet irradiance. With the chemistry-climate model (CCM) SOCOL[i] we have simulated the distribution of the temperature and gas species in the upper stratosphere and mesosphere driven by the daily measured and reconstructed SSI variability during January 2004. The obtained results open an opportunity for successful nowcast.

Nowcast of space weather has recently gained a lot of attention, because perturbations in solar activity can induce substantial changes in the Earth environment, which turn out to be important for space operations (Wilkinson, 1994), radio-wave propagation, GPS functionality and many other aspects of anthropogenic activity (Jansen et al., 2000).

We applied the chemistry-ionosphere-climate model SOCOL[i] (Egorova et al., 2010) to simulate the distribution of the temperature and gas species in the upper stratosphere and mesosphere. As an input for the simulation we exploit daily spectral solar irradiance measured by the SOLSTICE instrument onboard the SORCE spacecraft and reconstructed by Lean et al. (2005) for January 2004. We have carried out an ensemble of ten 1-month long simulations using slightly different initial states of the atmosphere. The boundary conditions and external forcing are identical for all ensemble members.

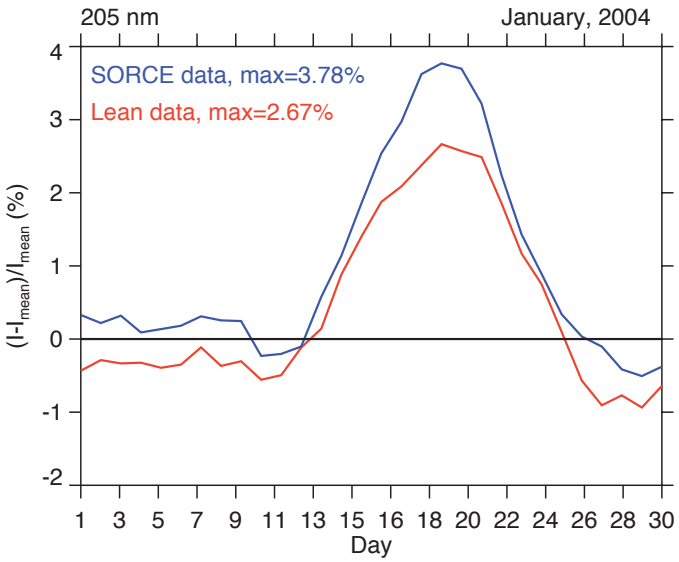

Figure 1. Relative deviation of the solar irradiance at 205 nm from its monthly mean for January 2004.

The solar irradiance variability at 205 nm during January 2004, which was used in the calculation, is illustrated in Figure 1. Solar activity during January 2004 was rather high and due to non-homogeneity in the distribution of Sun spots, the solar irradiance increased from January 11, reaching its maximum on January 19 and subsequently decreased until the end of January. Lean et al. (2005) and SOLSTICE data differ by ~1 % at the maximum.

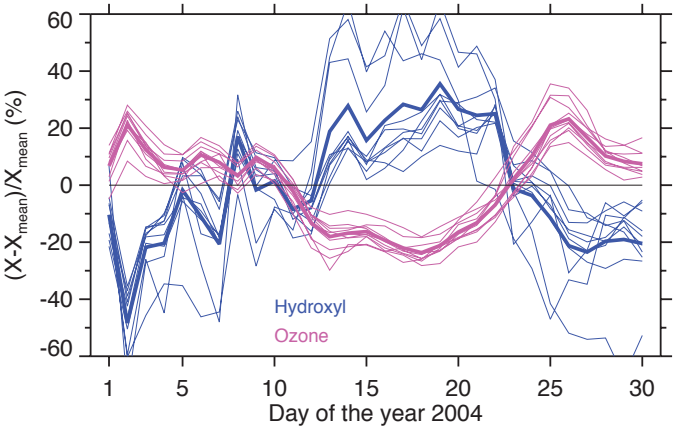

Figure 2. Relative deviation of hydroxyl and ozone at 80 km from its monthly mean for January 2004. Thick blue and pink lines show mean values of 10 member ensemble runs. The sensitivity of hydroxyl is multiplied by 10.

Figure 2 shows that hydroxyl and ozone in the mesosphere simulated with SOCOL[i] are sensitive to solar irradiance variability. In particular, the ensemble mean ozone and hydroxyl concentrations increase by 20 % and 3 % at the maximum of solar irradiance variability.

References:

Egorova T., Rozanov E., Ozolin Y., Shapiro A., Calisto M., Peter T., Schmutz W.: The atmospheric effects of October 2003 solar proton event simulated with the chemistry– climate model SOCOL using complete and parameterized ion chemistry. J. Atmos. Sol.-Terr. Phys., 2010.

Jansen F., Pirjola R., Favre R.: Space weather: Hazard to the Earth, Swiss Re Publishing, Zurich, 39 p, 2000.

Lean J., Rottman G., Harder J., Kopp G.: SORCE contributions to new understanding of global change and solar variability. Solar Physics, 230, 27-53, 2005.

Wilkinson D.C.: National Oceanic and Atmospheric Administration's spacecraft anomaly data base and examples of solar activity affecting spacecraft, J. Spacecraft and Rockets , Vol 31, March-April, 1994.

Effective Surface Albedo at Davos

Gregor Hülsen and Julian Gröbner

We describe a procedure to derive the effective surface albedo from cloud-free broadband UV irradiance measurements at Davos.

The effective surface albedo in 1-dimensional radiative transfer models (RTM) describes a nominal uniform surface albedo applied to the surface area to reproduce the observed incident UV irradiance (Weihs et al. 2001). The RTM used for the simulation is the widely used libRadtran package (Mayer and Kylling 2005). The following input parameters to the RTM are used for the calculation of cloud-free global UV irradiance:

- The total ozone column recorded by Brewer #163
- the spectral aerosol optical depth (AOD) from PFR measurements.

The effective surface albedo is then derived using the following procedure: First the algorithm chooses a cloud-free period using the APCADA algorithm (Dürr and Philipona 2004). Then, ancillary atmospheric parameters such as total column ozone and AOD are used as input parameters to the RTM to calculate simulated UV irradiances with the effective surface albedo as free parameter. The RTM calculations are iterated until the simulations agree with the local UV measurements. Negative values were set to a nominal albedo of 0.035, representative of snow-free surfaces.

The uncertainty of the derived effective surface albedo is mainly due to the uncertainties in the UV measurements and the uncertainties in the extraterrestrial spectrum used in the RTM. As shown by Gröbner et al. (2000) an uncertainty of ±4 % in the measured UV irradiance produces an uncertainty of ±0.1 in effective surface albedo. Based on the estimated uncertainty of the UV measurements of ±5 % we estimate the uncertainty in our derived effective surface albedo to be approximately ±0.15.

The effective surface albedo was calculated for the three years 2007-2009 (see Figure 1). In addition, we used daily snow height information provided by the Institute of Snow and Avalanches (SLF) to correlate with our calculations. As can be seen in Figure 1, in winter there is a permanent snow cover at Davos between the beginning of November until May. At Weissfluhjoch, located at 2540 m a.s.l., the snow cover extends until June or even July, which also influences the UV measurements at Davos and therefore the effective surface albedo.

In summer, the derived average effective albedo is 0.06 with a standard deviation of 0.04. Even in summer, episodes of snow fall can occur in Davos or in the surrounding mountains which increase the effective surface albedo for a short time to values comparable to the winter.

In winter, the average effective surface albedo is 0.53 with a standard deviation of 0.15. The high albedo in winter is due to the substantial snow cover in Davos and the surrounding area which is mostly above the tree line. This leads to an increase of the UV irradiance by 20 % in winter (assuming an effective albedo of 0.5) with respect to the snow-free situation (effective albedo 0.06).

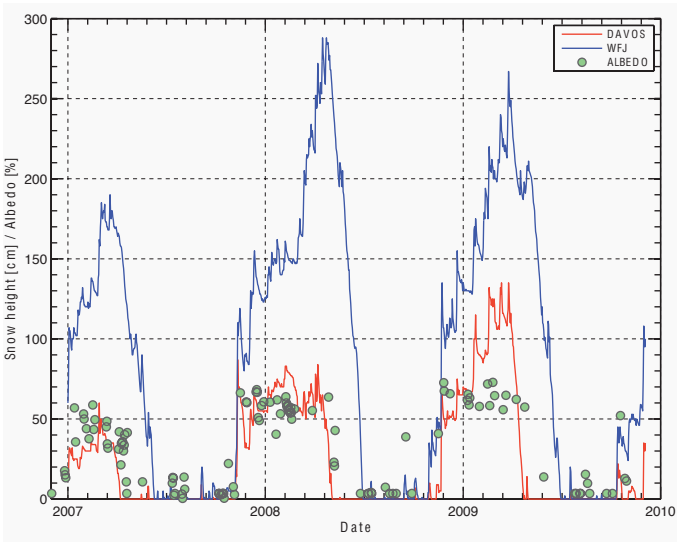

Figure 1. The snow height in centimeters is shown for Davos (red curve), and Weissfluhjoch-Messfeld (blue curve). The effective surface albedo derived for cloud-free days is shown by the green bullets in %.

References:

Weihs P., Lenoble J., Blumthaler M., Martin T., Seckmeyer G., Philipona R., De la Casiniere A., Sergent C., Gröbner J., Cabot T., Masserot D., Pichler T., Pougatch E., Rengarajan G., Schmucki D., Simic S.: Modeling the effect of an inhomogeneous surface albedo on incident UV radiation in mountainous terrain: determination of an effective surface albedo, Geophys. Res. Lett., 28, 3111-3114, 2001.

Mayer B., Kylling A.: Technical note: The libRadtran software package for radiative transfer calculations - description and examples of use, Atmos. Chem. Phys., 5, 1855-1877, 2005.

Dürr B., Philipona R.: Automatic cloud amount detection by surface longwave downward radiation measurements, J. Geophys. Res., 109 (D05201), 2004.

Gröbner J., Albold A., Blumthaler M., Cabot T., De la Casiniere A., Lenoble J., Martin T., Masserot D., Müller M., Philipona R., Pichler T., Pougatch E., Rengarajan G., Schmucki D., Seckmeyer G., Sergent C., Touré M.L., Weihs P.: Variability of spectral solar ultraviolet irradiance in an alpine environment, J. Geophys. Res., 105, 26991-27003, 2000.

Long-Term Trend Analysis of Cloud-Free Down-Welling Long-Wave Radiation from four Swiss Sites

Stefan Wacker and Julian Gröbner

We performed a long-term trend analysis of cloud-free down-welling long-wave radiation from four sites of the Alpine Surface Radiation Budget (ASRB) network. The study revealed positive but not significant trends.

The ASRB network was established in 1994/95 to assess surface radiative fluxes and their altitude dependence with high accuracy (Marty et al. 2002). We analyzed cloud-free down-welling long-wave radiation (DLRcf) from the ASRB stations Locarno-Monti (370 masl.), Payerne (490 masl.), Davos (1610 masl.), and Jungfraujoch (3580 masl.).

The cloud-free climatology was generated using the Automatic Partial Cloud Amount Detection Algorithm (APCADA) to separate cloud-free measurements. APCADA reliably detects low and middle clouds during night and day from down-welling long-wave radiation, air temperature and relative humidity at ground. However, it fails to detect thin cirrus clouds and thus, they are included in the cloud-free climatology. We applied the statistical approach described in Yue et al. (2002) to analyze the de-seasonalized monthly dataset. This method considers serial correlation and the potential interaction between a trend and the serial correlation. Results revealed positive trends ranging from 1 Wm^{-2}/dec at Jungfraujoch to 4.5 Wm^{-2}/dec at Davos and Payerne. However, none of the trends is statistically significant on the 95 % level. The increase in cloud-free down-welling long-wave radiation follows the trends in air temperature and specific humidity which have increased by about 1 °C/dec and 0.1 gkg^{-1}/dec, respectively.

Furthermore, we studied the trends in the single months. The results show distinctive trends in magnitude and sign (Figure 1). The trends tend to be negative or close to zero from December to March, while they are positive or close to zero from April to November. A remarkable exception is August where the trends are negative at all four stations. The signs of the slopes of all stations are in agreement and also follow the detected trends in air temperature and humidity. This consistent appearance of the trend pattern gives strong evidence that the trends are of regional origin and not locally induced.

We also calculated the down-welling long-wave radiation using the cloud-free parameterization of Brutsaert in order to attribute the cause of the changes in DLRcf. Thereby, we used the modified Brutsaert formula which accounts for the lapse rate in the atmospheric boundary layer (Gröbner et al. 2009). Results indicate that a large part of the observed trends can be explained by temperature and humidity changes. These changes might be caused by alterations in the circulation pattern. Finally, this analysis implies long-term changes in the cirrus cloud cover in some individual months.

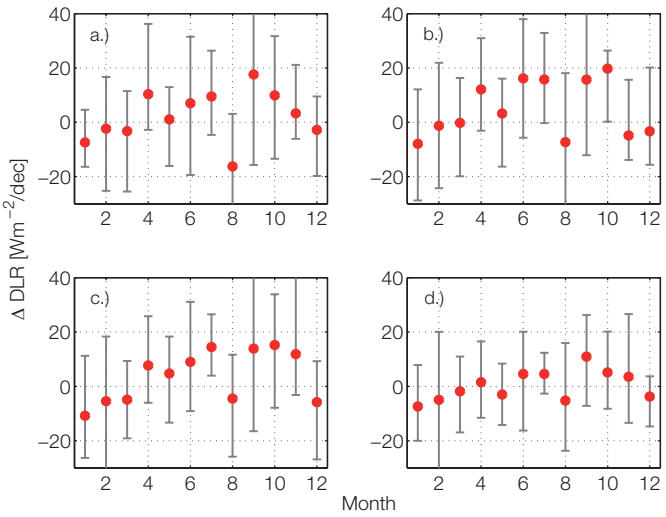

Figure 1. Estimate of trend magnitude (red points) in Wm^{-2} per decade with corresponding 95 % confidence interval of DLRcf: a.) Locarno-Monti, b.) Payerne, c.) Davos, d.) Jungfraujoch. A trend is significant if the corresponding confidence level does not span zero.

References:

Gröbner J., Wacker S., Vuilleumier L., Kämpfer N.: Effective atmospheric boundary layer temperature from longwave radiation measurements, J. Geophys. Res., 114(D19116), 2009.

Marty Ch., Philipona R., Fröhlich C., Ohmura A.: Altitude dependence of surface radiation fluxes and cloud forcing in the alps: results from the alpine surface radiation budget network, Theor. Appl. Climatol., 72, 137-154, 2002.

Yue S., Pilon P., Phinney B., Cavadias G.: The influence of autocorrelation on the ability to detect trend in hydrological series, Hydrol. Process., 16, 1807-1829, 2002.

NLTE Solar Irradiance Modeling with the COSI Code

Alexander Shapiro, Werner Schmutz, Micha Schoell, and Eugene Rozanov

We present a further development of the COde for Solar Irradiance (COSI) that now incorporates the calculation of molecular lines. The improved version of COSI allows us to reach a good agreement between the calculated and observed solar spectrum as measured by SOLSTICE and SIM onboard the SORCE satellite. We demonstrate that Non Local Thermodynamic Equilibrium (NLTE) effects are very important for the modeling of the solar spectrum even in the visual part of the spectrum and for its variability over the entire solar spectrum.

COSI accounts for the explicit NLTE effects in several hundred lines, while the NLTE effects in the other several millions lines are indirectly included via an iterated opacity distribution function (Haberreiter et al. 2008).

Several adjustments of the code were conducted to reach better agreement with observed spectra. The two most important improvements were the inclusion of molecular lines and the introduction of additional opacity, which probably arises from the unknown lines. The calculation of the molecular lines gives good agreement with the SORCE observations in the main molecular bands (especially in the CN violet system and CH G band), while the additional opacity allows us to solve the well-known problem of overestimation of the UV flux in the synthetic spectrum.

In Fig. 1 we present the solar spectrum calculated with the FALC99 atmosphere model from Fontenla et al. (1999) compared with the SORCE measurements. One can see that, excluding the short wave region, where we are missing the proper NLTE treatment of several strong lines, the overall agreement is very good. The Ly α line is already computed in NLTE and we obtain an overestimation of its flux. In a forthcoming paper we will investigate this in more detail (Schoell et al. 2010).

Fig. 2 shows the flux differences between the active components of the solar atmosphere and the quiet Sun calculated in LTE and NLTE. The most prominent peak at about 3890 Å corresponds to the CN violet system. Although the differences in the CH G band around 4300 Å are also clearly visible, they are less pronounced than in the CN violet system. This is mainly due to the differences in the CH and CN dissociation energies (3.465 eV and 7.76 eV), so the CN concentration is more sensitive to temperature variations. Furthermore, the contrast between the active components and the quiet Sun is significantly decreased in the NLTE calculations. As a consequence the NLTE calculations reduce the solar variability in the visible and IR, shifting the variability to the UV. As the corrected NLTE calculations do not change the visible and IR continuum they are free from this effect.

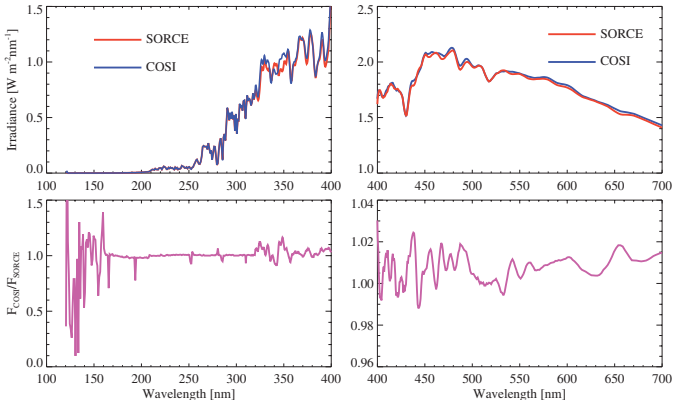

Figure 1. Upper panel: SORCE observations vs. COSI calculations. Lower panel: ratio between the calculations and measurements.

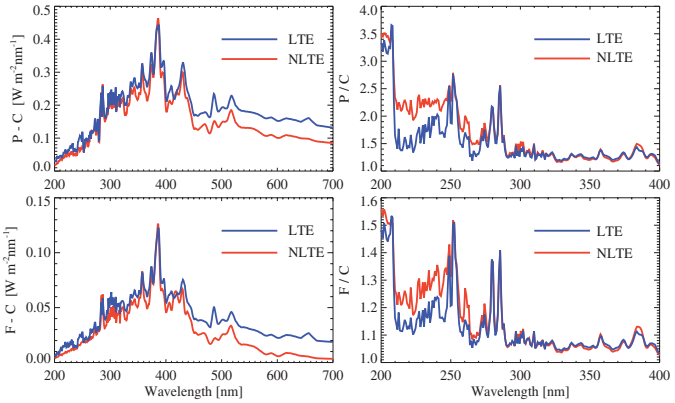

Figure 2. The flux differences between plage and quiet Sun (upper panel) and bright network and quiet Sun (lower panel) calculated in NLTE and LTE.

References: Fontenla J., White O.R., Fox P. A., Avrett E.H., Kurucz R.L.: Calculation of Solar Irradiances I. Synthesis of the Solar Spectrum, ApJ, 518, 480, 1999.

Haberreiter M., Schmutz W., Hubeny I.: NLTE model calculations for the solar atmosphere with an iterative treatment of opacity distribution functions, Astron. Astrophys., 492, 833, 2008.

Schoell M., Schmutz W., Haberreiter M., Shapiro A., 2010, A&A, in preparation.

The Shape of the Solar Limb

Alexander Shapiro and Werner Schmutz in collaboration with Gerard Thuillier, LATMOS, Verrieres le Buisson, France

We employ the COde for Solar Irradiance (COSI) to calculate the shape of the solar limb. We show that the contribution from spectral lines can significantly change the limb profile and increase the observed solar radius.

SOlar Diameter Imager and Surface Mapper (SODISM) onboard the PICARD satellite, which is to be launched in early 2010, will observe the solar limb with a high cadence and precision. To assist the interpretation of future data several radiative radiative transfer codes (SRPM, PHOENIX, Mein models) were compared (Thuiller et al. 2010). We contributed to this project with COSI, developed at PMOD/WRC.

At the limb the optical depth of the solar atmosphere steeply decreases and becomes optically thin. It results in the drop of the emerged intensity over the entire solar spectrum. However the photons at different wavelengths originate in different layers of the solar atmosphere so that the profile of this drop strongly depends on the wavelength. Strong spectral lines usually have a significant chromospheric contribution which shifts the position of the inflection point to the outer level of the solar atmosphere and increases the observed solar radius. The chromospheric contribution is usually stronger in the warmer parts of the solar atmosphere (bright network or plage) so they correspond to a larger solar radius. These effects are illustrated in Fig. 1 where the limb profiles at the Ca II K line and at the wavelength 535.7 nm are plotted for different solar atmosphere models. One can also see that the increase of the solar radius in the Ca line is much stronger than in the continuum.

In Fig. 2. we illustrate the influence of the spectral lines on the solar radius. One can see that the position of the inflection point moves outward with increasing wavelength. In the presence of the spectral lines, the chromospheric radiation displaces the inflection point outwards by a very large amount.

To illustrate the choice of the wavelength for the PICARD continuum channel (607 nm, width is 0.8 nm), COSI was run at high resolution in its domain. The result is shown in Fig. 3. One can see that the overall effect of the spectral lines is quite small.

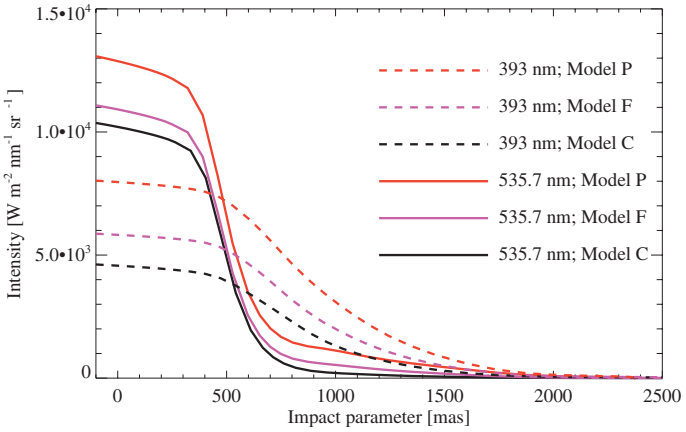

Figure 1. The solar limb profile calculated for the plage (Model P), the bright network (Model F) and the quiet Sun (Model C) at Ca II K line (393 nm) and at one of the PICARD channels (535.7 nm) which is free from strong lines.

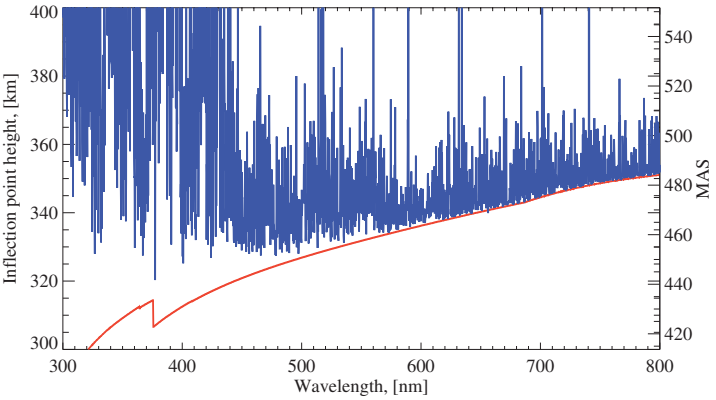

Figure 2. The position of the inflection point as a function of wavelength for the calculations with and without spectral lines.

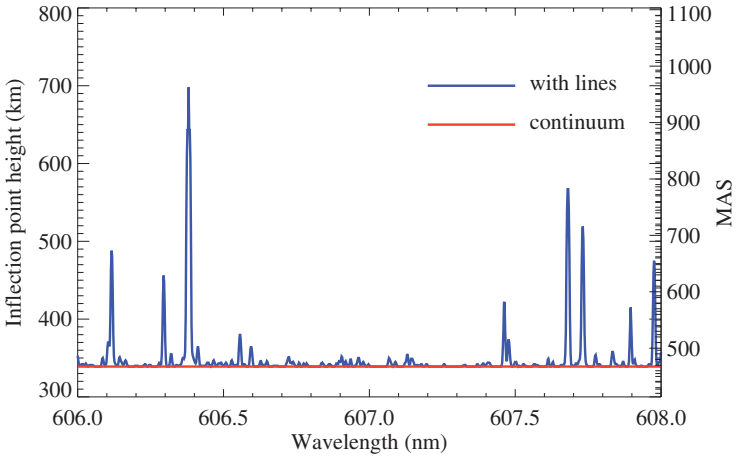

Figure 3. The position of the inflection point as a function of wavelengths at high resolution for calculation with and without spectral lines in the spectral region of one of the PICARD channels.

References: Thuillier G., Claudel J., Djafer D., Haberreiter M., Mein N., Melo S., Schmutz W., Shapiro A., Short I., Sofia S.: The shape of the solar limb: theory and observations. Solar Physics, 2010, submitted.

TSI and SSI Reconstruction back to the Maunder Minimum

Alexander Shapiro, Werner Schmutz, Micha Schoell, and Eugene Rozanov in collaboration with EAWAG

We apply the COde for Solar Irradiance (COSI) to reconstruct the Total Solar Irradiance (TSI) and Spectral Solar Irradiance (SSI) back to the Maunder minimum on the basis of sunspot numbers and ^{10}Be data.

While solar irradiance variability over an 11-year cycle can be directly observed, there is no unambiguous way to measure the secular trend (e.g. Solanki and Krivova 2004). This leads to a significant difference in the estimates of past TSI as published in recent literature studies.

We assume that today's quiet Sun consists of two components. The first corresponds to the average quiet network and it is responsible for all magnetic activity of the quiet Sun. The second represents the Sun that is basically free from any magnetic activity. We use the open magnetic flux data reconstructed by Steinhilber et al. (2010) to determine the filling factors of these components. Then we use sunspot numbers to reconstruct filling factors of the solar active components (plage, bright network and sunspots). The TSI and SSI contributions from every component are calculated with COSI (Shapiro et al. 2010). The comparison of the reconstructed TSI with the PMOD composite is given in Fig.1, while the reconstruction back to the Maunder minimum is presented in Fig. 2. One can see that these basic assumptions lead to a TSI and SSI that was substantially different during the Maunder minimum than as it is observed today. The differences are especially strong in the UV, however due to the presence of the strong variable (e.g. molecular) lines they can also be significant in the visible part of the spectrum (see fourth panel of Fig. 2).

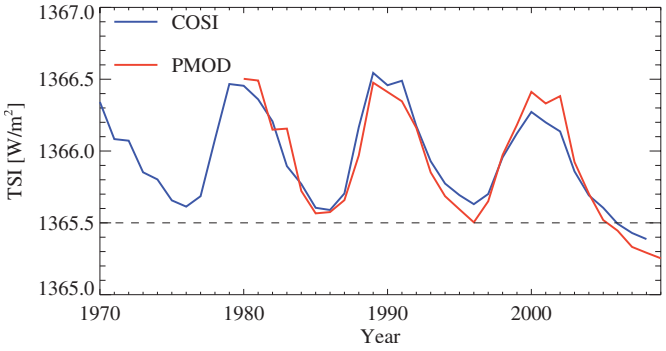

Figure 1. Upper panel: Reconstructed with COSI code TSI (blue curve) vs. PMOD composite (red curve). Lower panel: evolution of the sunspot filling factor with time.

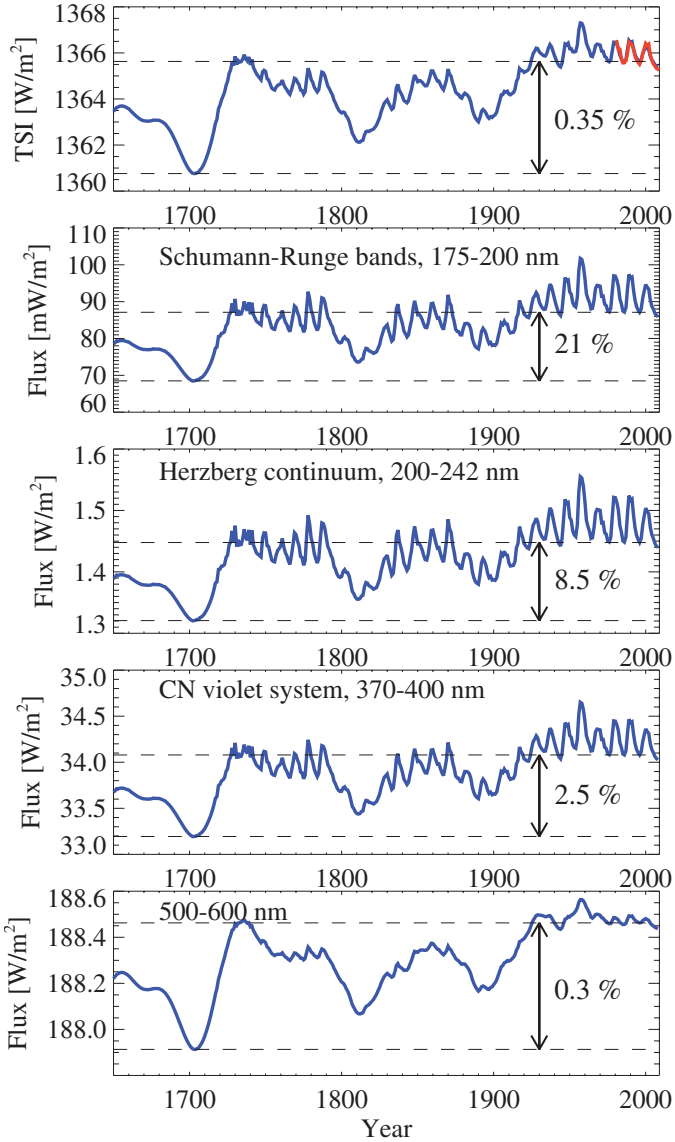

Figure 2. Reconstructed (blue) and observed (red) TSI as well as SSI in several spectral bands.

References:

Solanki S.K., Krivova N.: Solar irradiance variations: Current measurements to long-term estimates. Solar Phys. 224, 197 – 208, 2004.

Shapiro A., Schmutz W., Schoell M., Haberreiter M., Rozanov E.: NLTE Solar Irradiance Modeling with the COSI code, Astron. and Astophys., submitted, 2010.

Steinhilber F., Abreu J.A., Beer J., McCracken K.G.: Interplanetary magnetic field during the past 9300 years inferred from cosmogenic radionuclides. Journal of Geophysical Research, 115, A01104, 2010.

Evidence of Solar Cycle Velocity Amplitude Changes Consistent with Mode Conversion Theory

Rosaria Simoniello and Wolfgang Finsterle

We investigated the induced solar cycle changes in p-mode velocity amplitudes in the attempt to link these variations to slow and fast MHD waves.

We have used long duration, high quality, unresolved (Sun-as-a star) line-of-sight velocity and continuum intensity observations to search for solar cycle related change in oscillatory amplitudes for the frequency range 2.5<ν<6.8 mHz. The line-of-sight velocity data were collected by the ground based network BiSON (Birmingham Solar Oscillation Network) and by the instrument GOLF (Global Oscillation at Low Frequency), on board the ESA/NASA SOHO satellite. The continuum intensity measurements are provided by SOHO/VIRGO (Variability of Irradiance and Gravity Oscillations).

Over the ascending phase of solar cycle 23 we found a suppression in p-mode amplitudes in both velocity data sets between 2.5<ν<4.5 mHz with maximum suppression for frequencies in the range 2.5<ν<3.5 mHz. The size of the amplitude suppression is 13±2 and 9±2 per cent for intensity observations. Over the range 4.5<ν<5.5 mHz the findings hint, within the errors, to a null change. At still higher frequency, in the so called High-frequency Interference Peaks (HIPs), between 5.8<ν<6.8 mHz, we found an enhancement in the velocity amplitudes, with the maximum, 36±7 per cent, occurring for 6.3 <ν< 6.8 mHz.

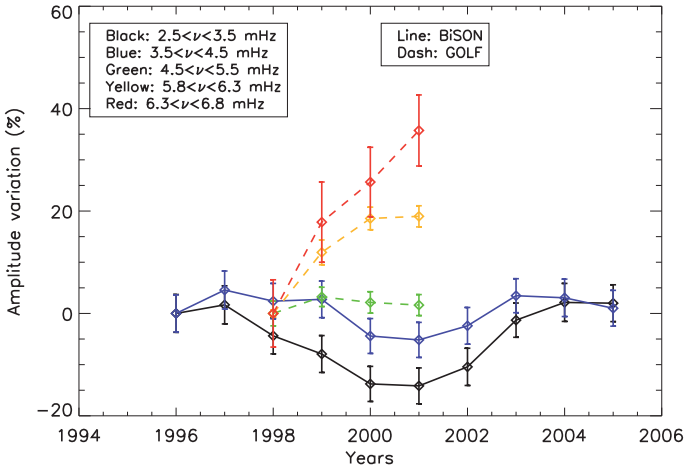

Figure 1. Solar cycle changes in the p and HIPs band from BiSON and GOLF observations. The different colors identify the 5 frequency intervals.

The novelty of this investigation is the simultaneous observation of low-frequency acoustic absorption and high-frequency enhancement. The frequency dependence of solar-cycle velocity amplitude changes has been shown to be consistent with transmission from acoustic to slow-magnetoacoustic waves occurring in non-vertical magnetic field (Simoniello et al. 2010).

Strong surface magnetic fields allow the initial internal acoustic wave energy to be split into fast and slow magnetoacoustic modes. This splitting has to satisfy the following conservation wave energy: fast energy + slow energy = total energy. The transmission coefficient, T, is defined as the amount of energy transmitted from internal acoustic-to-slow or slow-to-internal acoustic waves during mode transmission. It has been shown that for the same magnetic field strength and inclination, T is smaller for higher frequencies (Schunker et al. 2006). This implies that (in the interior of the Sun) the transmission from internal acoustic to slow magnetoacoustic waves becomes less dominant with increasing frequency.

Our observations found a maximum suppression of power between 2.5<ν<3.5 mHz, possibly caused by slow magnetoacoustic waves traveling upwards. Therefore, from mode conversion theory, it may be the case that the field inclination is of the order of 60° to allow the resonant modes to be transmitted predominantly as slow-magnetoacoustic waves traveling outwards from the photosphere. For higher frequencies, between 3.5<ν<4.5 mHz and for the same field inclination, the transmission coefficient is slightly smaller in agreement with the reduced acoustic power suppression found in the 2nd p-band. In the 3rd p-band the transmission coefficient gets even smaller allowing the resonant modes to be split almost equally between the slow and the fast component. This is in agreement with the almost null suppression found in the 3rd-p-band. At 60° field inclination, the internal acoustic waves, above 6 mHz, retain their fast nature. In this case, the two restoring forces acting to generate the fast magnetoacoustic mode (gas pressure and magnetic pressure fluctuations) are in phase and add constructively for the fast mode increasing the acoustic power. Therefore, we observe a change in the sign of the integrated acoustic power above the 5mHz with a maximum occurring between 6.3<ν<6.8mHz.

These findings have a strong implication for the better understanding of the role played by waves in chromospheric heating. While fast magnetoacoustic are refracted backwords, slow-magnetoacoustic waves can travel in the atmosphere. Thus the latter could play a major role in the chromospheric heating of magnetized areas.

References: Schunker H., Cally P.S., MNRAS, 372, 551, 2006.

Simoniello R., Finsterle W., Garcia R.A., Salabert D., Jimenez A., Elsworth Y., Schunker H., A&A, in press, 2010.

Reconstruction of a Century of Broadband Atmospheric Transmission using Historic and Contemporary Pyrheliometer Measurements

Daniel Lachat and Christoph Wehrli

We extract pyrheliometer data from various sources within the PMOD/WRC archive which reaches back to 1909. In order to calculate a time-series of broadband apparent atmospheric transmission we apply the Rationing Technique used by Hoyt and Fröhlich (1983).

Solar radiation and atmospheric transmission have been of increasing interest in climate research in the past decades. In this context, recent studies have observed decadal trends in solar radiation incident at the Earth's surface. These claim a decrease of solar irradiance starting from the 1950s to the end of the 1980s followed by an increase from the 1990s to present. These periods are referred to as Global Dimming and Global Brightening, respectively (Ohmura and Wild, 2005). Trends in cloud coverage and atmospheric transmission are prime focal points in the quest for possible causes of this variability.

We are currently digitizing historic measurements taken with various instruments from 1909 to the present, and are homogenizing the radiometric scales in use to the World Radiometric Reference (WRR).

The measurement time is converted to optical air mass which is defined as the length of a radiation path through the atmosphere relative to the zenith. Following the rationg technique used by Hoyt and Fröhlich (1983), apparent atmospheric transmission is obtained by calculating the ratio of two fixed air masses which requires inter,- and extrapolation of the measured irradiance values. The data is therefore fitted to a parabolic or an exponential function respectively. The adequacy of this fit is crucial to the determination of the irradiances at the desired air masses. The performance of the chosen fitting functions is compared and suitable criteria for the selection of raw data will be established.

A first overview of the transmission time-series covering the period 1909-1969 has shown fair agreement with the results published by Hoyt and Fröhlich (1983). No significant trend in apparent transmission found during this period with quite some remarkable consistency. Discrepancies are thought to have their origin in different methods for the selection of raw data. Further investigation of the complete time-series will also provide information on the trend in atmospheric transmission during the Global Dimming/Brightening transition from 1970 to 1990.

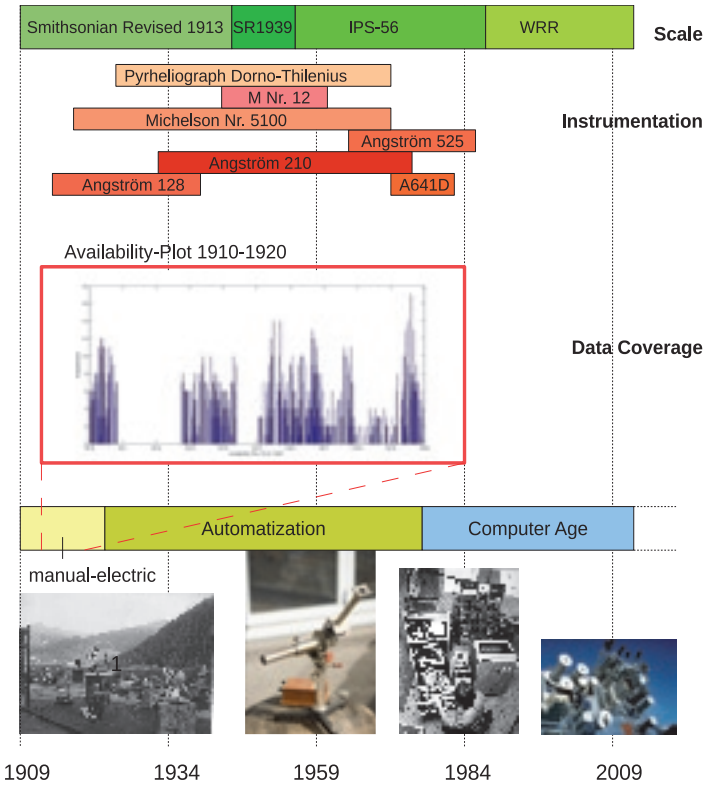

Figure 1. Overview of the measurement-series. Different measurement scales and instrumentation which correspond to their respective time period are homogenized. Data coverage is shown as number of measurements per day from 1910 to 1920.

References: Ohmura A., Wild M.: From dimming to brightening: Decadal changes in surface solar radiation, Science 308, 847-850, 2005.

Hoyt D., Fröhlich C.: Atmospheric Transmission at Davos 1909-1979, Climate Change 5, 61-71, 1983.

PMO6-type Radiometer Calibration at the Total Solar Irradiance Facility at the Laboratory for Atmospheric and Space Physics in Boulder

André Fehlmann, Wolfgang Finsterle, and Werner Schmutz in collaboration with LASP, USA

We compared two PREMOS radiometers and a VIRGO spare PMO6-type radiometer with the cryogenic absolute radiometer at the Total Solar Irradiance Facility (TRF). The power comparison confirmed the calibration performed in 2008 at the National Physical Laboratory in London.

Final thermal tests of the PREMOS/PICARD package revealed an unstable heater resistor in the designated flight instrument PREMOS-1. Although the radiometer still measures correctly, we decided to replace it with spare instrument PREMOS-3. Prior to the exchange, we had the possibility to calibrate PREMOS-3 at the TRF.

From the 6th until the 23rd July 2009 we performed power, irradiance and air-to-vacuum comparisons between the VIRGO spare, the PREMOS-3 and the SI traceable cryogenic radiometer at the TRF. The precision aperture under filling power measurements showed that the instruments read 0.7 % (VIRGO) respectively 0.63 % (PREMOS-3) higher than the SI scale. Because both absolute radiometers were fully characterized, we have to find an explanation for this as yet un-described effect. We think that the most plausible reason for the offset is a high ohmic short circuit in the radiometer heater circuit. This will be further investigated with other instruments that behave in a similar manner.

The irradiance comparison has not been evaluated as the TRF radiometer aperture area has not yet been measured. However, another interesting phenomena was discovered which had not been previously observed. First, the radiometers measured the irradiance of a 7.3 mm diameter beam over-filling the precision aperture. Then we enlarged the beam to 11mm which over-fills all apertures of the radiometer. Although we corrected for the diffraction at the view limiting aperture, we found an offset of 0.25 % (VIRGO) respectively 0.14 % (PREMOS-3) for the larger beam. A possible explanation for this effect could be stray-light from the land of the view limiting aperture. This could possibly explain part of the 0.35 % discrepancy between the VIRGO/SOHO and the TIM/SOURCE experiments.

After the substitution, we also took the PREMOS-1 radiometer to the TRF from 5th to 7th October 2009. The power comparison confirmed the NPL calibration, i.e. PREMOS-1 measured 0.05 % less than the SI scale. In addition, a stray-light effect that amounts to 0.2 % was found.

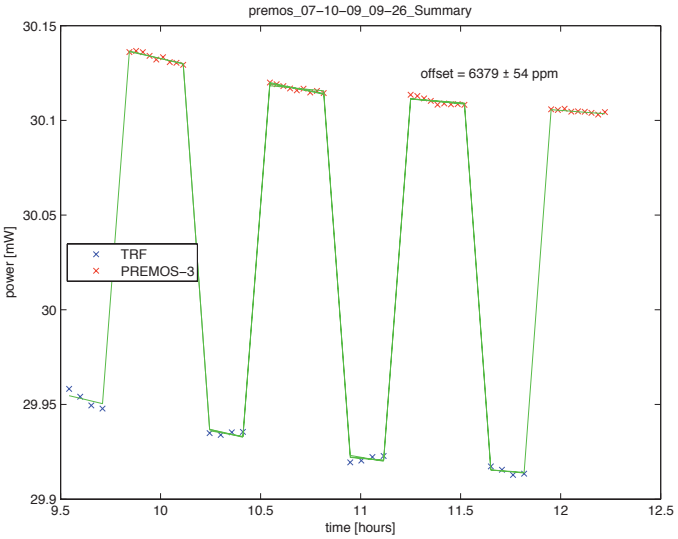

Figure 1. The evaluation of the PREMOS-3 power comparison with the TRF cryogenic radiometer shows that PREMOS-3 reads 0.63 % higher than the SI scale.

Currently, we are conducting tests to ensure that no other effects influence measurements at the TRF as the irradiance beam is formed by spirally scanning a small laser beam. We are concerned about the high local power density in the beam which may produce different aperture heating than for solar radiation. Second, we are fairly sure that the diffraction correction applied for the sun does not hold for a small gaussian beam scanning over the apertures.

References: Kopp G., Heuerman K., Harber D., Drake G.: The TSI Radiometer Facility: absolute calibrations for total solar irradiance instruments, Earth Observing Systems XII, 1, 6677, 2007.

Schmutz W., Fehlmann A., Hülsen G., Meindl P., Winkler R., Thuillier G., Blattner P., Buisson F., Egorova T., Finsterle W., Fox N., Gröbner J., Hochedez J.-F., Koller S., Meftah M., Meisonnier M., Nyeki S., Pfiffner D., Roth H., Rozanov E., Spescha M., Wehrli C., Werner L., Wyss J.U.: The PREMOS/PICARD instrument calibration, Metrologia 46, S202-S206, 2009.

Publications

Refereed Publications

Appourchaux T., Liewer P., Watt M., Alexander D., Andretta V., Auchere F., D'Arrigo P., Ayon J., Corbard T., Fineschi S., Finsterle W., Floyd L., Garbe G., Gizon L., Hassler D., Harra L., Kosovichev A., Leibacher J., Leipold M., Murphy N., Maksimovic M., Martinez-Pillet V., Matthews B. S.A., Mewaldt R., Moses D., Newmark J., Regnier S., Schmutz W., Socker D., Spadaro D., Stuttard M., Trosseille C., Ulrich R., Velli M., Vourlidas A., Wimmer-Schweingruber C. R., Zurbuchen T.: 2009, POLAR Investigation of the Sun – POLARIS, Experimental Astronomy 23, 1079-1117, doi:10.1007/s10686-008-9107-8.

Austin J., Wilson R.J., Akiyoshi H., Bekki S., Butchart N., Claud C., Fomichev V.I., Forster P., Garcia R.R., Gillett N.P., Keckhut P., Langematz U., Manzini E., Nagashima T., Randel W.J., Rozanov E., Shibata K., Shine K.P., Struthers H., Thompson D.W.J., Wu F., Yoden S.: 2009, Coupled chemistry climate model simulations of stratospheric temperatures and their trends for the recent past, Geophys. Res. Lett., 36, L13809, doi:10.1029/2009GL038462.

BenMoussa A., Dammasch I.E., Hochedez J.-F., Schühle U, Koller S., Stockman Y., Scholze F., Richter M., Kroth U., Laubis C., Dominique M., Kretzschmar M., Mekaoui S., Gissot S., Theissen A., Giordanengo B., Bolsee D., Hermans C., Gillotay D., Defise J.M., Schmutz W.: 2009, Pre-flight calibration of LYRA, the solar VUV radiometer on board PROBA2, A&A 508, 1085-1094, doi: 10.1051/0004-6361/200913089.

Brönnimann S., Stickler A., Griesser T., Ewen T., Grant A.N., Fischer A.M., Schraner M., Peter T., Rozanov E., Ross T.: 2009, Exceptional atmospheric circulation during the "Dust Bowl", Geophys. Res. Lett., 36, L08802, doi:10.1029/2009GL037612.

Brönnimann S., Stickler A., Griesser T., Fischer A., Grant A., Ewen T., Zhou T., Schraner M., Rozanov E., Peter T.: 2009, Variability of large-scale atmospheric circulation indices for the northern hemisphere during the past 100 years, Meteorologische Zeitschrift, 18, 4, 379-396.

Cachorro V.E., Berjon A., Toledano C., Mogo S., Prats N., de Frutos A.M., Vilaplana J.M., Sorribas M., de la Morena B.A., Gröbner J., Laulainen N.: 2009, Detailed Aerosol Optical Depth Intercomparison between Brewer and Li-Cor 1800 Spectroradiometers and a Cimel Sun PhotometerJ. Atmos. Ocean. Tech., 26, 1558-1571, doi: 10.1175/2009JTECHA1217.1.

Cagnazzo C., Manzini E., Calvo N., Douglass A., Akiyoshi H., Bekki S., Chipperfield M., Dameris M., Deushi M., Fischer A., Garny H., Gettelman A., Giorgetta M.A., Plummer D., Rozanov E., Shepherd T.G., Shibata K., Stenke A., Struthers H., Tian W.: 2009, Northern winter stratospheric temperature and ozone responses to ENSO inferred from an ensemble of Chemistry Climate Models, Atmos. Chem. Phys., 9, 8935-8948.

Domingo V., Ermolli I., Fox P., Fröhlich C., Haberreiter M., Krivova N., Kopp G., Schmutz W., Solanki S.K., Spruit H.C., Unruh Y., Vögler A.: 2009, Solar Surface Magnetism and Irradiance on Time Scales from Days to the 11-Year Cycle, Space Sci. Rev. 145, 337-380, doi: 10.1007/s11214-009-9562-1.

Fröhlich C.: 2009, Evidence of a long-term trend in total solar irradiance. Astron. Astrophys., L27-L30, doi: 10.1051/0004-6361/200912318.

Fröhlich C.: 2009, Total Solar Irradiance Variability: What have we learned about its Variability from the Record of the last three Solar Cycles? In: T. Tsuda, R. Fujii, K. Shibata, and M.A. Geller, editors, Climate and Weather of the Sun-Earth System (CAWSES): Selected Papers from the 2007 Kyoto Symposium, pages 217-230, Setagaya-ku, Tokyo, Japan. Terra Publishing.

Gettelman A., Birner T., Eyring V., Akiyoshi H., Plummer D.A., Dameris M., Bekki S., Lefevre F., Lott F., Bruehl C., Shibata K., Rozanov E., Mancini E., Pitari G., Struthers H., Tian W., Kinnison D.E.: 2009, The Tropical Tropopause Layer 1960-2100, Atmos. Chem. Phys., 9, 1621-1637.

Refereed Publications

Gröbner J., Wacker S., Vuilleumier L., Kämpfer N.: 2009, Effective atmospheric boundary layer temperature from longwave radiation measurements, J. Geophys. Res., 114, D19116, doi:10.1029/2009JD012274.

Heckendorn P., Weisenstein D., Fueglistaler S., Luo B.-P., Rozanov E., Schraner M., Thomason L., Peter T.: 2009, The impact of geoengineering aerosols on stratospheric temperature and ozone, Environ. Res. Lett., 4, doi: 10.1088/1748-9326/4/4/045108.

Kucharski A., Scaife A., Yoo J.H., Folland C.K., Kinter J., Knight J., Fereday D., Fischer A.M., Jin E.K., Krueger J., Lau N.-C., Nakaegawa T., Nath M.J., Pegion P., Rozanov E., Schubert S., Sporyshev P.V., Syktus J., Voldoire A., Yoon J.H., Zeng N., Zhou T.: 2008, The CLIVAR C20C Project. Skill of simulating Indian monsoon rainfall on interannual to decadal timescale. Does GHG forcing play a role?, Clim. Dyn, 33, 615-627, doi:10.1007/s00382-008-0462-y.

Ozolin Y., Karol I., Rozanov E., Egorova T.: 2009, A Model of the Impact of Solar Proton Events on the Ionic and Gaseous Composition of the Mesosphere, Izvestiya, Atmospheric and Oceanic Physics, 45, 6, 737-750.

Scarnato B., Staehelin J., Peter T., Gröbner J., Stübi R.: 2009, Temperature and slant path effects in Dobson and Brewer total ozone measurements, J. Geophys. Res., 114, D24303, doi:10.1029/2009JD012349.

Schmutz W., Fehlmann A., Hülsen G., Meindl P., Winkler R., Thuillier G., Blattner P., Buisson F., Egorova T., Finsterle W., Fox N., Gröbner J., Hochedez J.-F., Koller S., Meftah M., Meisonnier M., Nyeki S., Pfiffner D., Roth H., Rozanov E., Spescha M., Wehrli C., Werner L., Wyss J.U.: 2009, The PREMOS/PICARD instrument calibration, Metrologia 46, S202-S206, doi: 10.1088/0026-1394/46/4/S13.

Seppälä A., Randall C.E., Clilverd M.A., Rozanov E., Rodger C.J.: 2009, Geomagnetic activity and polar surface air temperature variability, J. Geophys. Res., 114, A10312, doi:10.1029/2008JA014029.

Son S.-W., Polvani L., Waugh D., Birner T., Akiyoshi H., Garcia R., Gettelman A., Plummer D., Rozanov E.: 2009, The Impact of Stratospheric Ozone Recovery on Tropopause Height Trends, J. of Climate, 22, 429-445, doi: 10.1175/2008JCLI2215.1.

Steinhilber F., Beer J., Fröhlich C.: 2009, Total Solar Irradiance During the Holocene, Geophys. Res. Lett., 36, L19704, doi: 10.1029/2009GL040142.

Struthers H., Bodeker G., Austin J., Bekki S., Cionni I., Dameris M., Giorgetta M.A., Grewe V., Lefevre F., Lott F., Manzini E., Peter T., Rozanov E., Schraner M.: 2009, The simulation of the Antarctic ozone hole by chemistry-climate models, Atmos. Chem. Phys., 9, 6363-6376.

Struthers H., Bodeker G.E., Smale D., Rozanov E., Schraner M., Peter T.: Evaluating how photochemistry and transport determine stratospheric inorganic chlorine in coupled chemistry-climate models, Geophys. Res. Lett., 36, L04805, doi: 10.1029/2008GL036403.

Tourpali K., Bais A.F., Kazantzidis A., Zerefos C.S., Akiyoshi H., Austin J., Brühl C., Butchart N., Chipperfield M.P., Dameris M., Deushi M., Eyring V., Giorgetta M.A., Kinnison D.E., Mancini E., Marsh D.R., Nagashima T., Pitari G., Plummer D.A., Rozanov E., Shibata K., Tian W.: 2009, Clear sky UV simulations in the 21st century based on ozone and temperature projections from Chemistry-Climate Models, Atmos. Chem. Phys., 9, 1165-1172.

Turck-Chièze S., Lamy P., Carr C., Carton P.H., Chevalier A., Dandouras I., Defise J.M., Dewitte S., Dudok de Wit T., Hasan S., Hochedez J-F., Horbury T., Levacher P., Meissonier M., Murphy N., Rochus P., Ruzmaikin A., Schmutz W., Thuillier G., Vivès S.: 2009, The DynaMICCS perspective, Experimental Astronomy 23, 1017-1055, doi: 10.1007/s10686-008-9111-z.

Zhou T., Bo Wu, Scaife A., Brönnimann S., Cherchi A., Fereday D., Fischer A., Folland C., Jin K., Kinter J., Knight J., Kucharski F., Kusunoki S., Lau N.-C., Lijuan Li, Nath M., Nakaegawa T., Navarra A., Pegion P., Rozanov E., Schubert S., Sporyshev P., Voldoire A., Xinyu Wen, Yoon J., Zeng N.: 2009, The CLIVAR C20C project: which components of the Asian-Australian monsoon circulation variations are forced and reproducible? Clim. Dyn., 33, 1051-1068, doi: 10.1007/s00382-008-0501-8.

Other Publications

Dominique M., Gillotay D., Fussen D., Vanhellemont F., Hochedez J.-F., Schmutz W.: 2009, The Contribution of PROBA2-LYRA Occultations to Earth Atmosphere Composition Analysis. In: New Horizons in Occultation Research: Studies in Atmosphere and Climate, A. Steiner, B. Pirscher, U. Foelsche, and G. Kirchengast (eds.), Springer Berlin Heidelberg, p. 283-292.

Gröbner J., Hülsen G.: 2009, The quality assurance program for spectral UV measurements in Europe. In: Proc. MOCA 09 Joint Assembly, 19-29 July 2009, Montreal, Canada.

Gröbner J., Hülsen G., Vuilleumier L., Blumthaler M., Vilaplana J.M., Walker D., Gill J.E.: 2009, COST Action 726 – Report of the PMOD/WRC–COST Calibration and Intercomparison of Erythemal Radiometers, COST Office, PMOD/WRC internal publication 1113.

Gröbner J., Wacker S. Vuilleumier L.: 2009, Effective boundary layer temperature from atmospheric water vapour emission. In: General Assembly EGU, G. Res. Abs., 11, 10014.

Hülsen G.: 2009, Verstärkt Wasser die ultraviolette Strahlung?, In: Graubünden – Das blaue Wunder, Ernst Bromeis-Camichel, 192-193, Südostschweiz Buchverlag.

Hülsen G., Gröbner J.: 2009, Measurement of the Vitamin D3 Dose using Broadband ultraviolet Radiometers. In: Proc. MOCA 09 Joint Assembly, 19-29 July 2009, Montreal, Canada.

Millour F., Chesneau O., Driebe T., Matter A., Schmutz W., Lopez B., Petrov R.G., Groh J.H., Bonneau D., Dessart L., Hofmann K.H., Weigelt G.: 2009, Wolf-Rayet Stars at the Highest Angular Resolution, The Messenger 135, 26-31.

Shapiro A.I., Fluri D.M., Berdyugina S.V., 2009, Solar Magnetic Field Diagnostics with the Molecular Hanle Effect, Solar Polarization 5. In: ASP Conference Series, Vol. 405, Edited by Svetlana V. Berdyugina, K. N. Nagendra, and Renzo Ramelli. San Francisco: Astronomical Society of the Pacific, p. 343.

Simoniello R., Finsterle W., Garcia R.A., Salabert D., Jiménez A.: 2009, Evidence of Increasing Acoustic Emissivity at High Frequency with Solar Cycle 23 in Sun-as-a-star Observations. In: AIPCS 1170, J.A. Guzik, P.A. Bradley, p. 566-568, doi: 10.1063/1.3246563.

Skinner S.L., Zhekov S., Guedel, M., Schmutz W., Sokal K.; 2009, A Survey of X-ray Emission from Wolf-Rayet Stars. In: AAS Meeting Abstracts 213, 491.20.

Wacker S., Gröbner J., Emde C., Vuilleumier L., Mayer B., Rozanov E.: Comparison of measured and modeled nocturnal clear sky longwave downward radiation at Payerne, Switzerland. In: Current problems in atmospheric radiation (IRS 2008): Proceedings of the International Radiation Symposium (IRC/IAMAS), AIP Conf. Proc, Volume 1100, p. 589-592, DOI:10.1063/1.3117055.

Wacker S., Gröbner J., Nowak D., Vuilleumier L. Kämpfer N.: Surface Longwave Cloud Radiative Forcing of Stratus Clouds at the BSRN site. Payerne, Switzerland. General Assembly EGU, G. Res. Abs., 11, 10787, 2009.

Wehrli C.: Improvement of Dissemination of Ozone and Aerosol observations through the WIS, CBS TECO Conference on WIGOS, 23-24 March 2009, Dubrovnik, Croatia. http://www.wmo.int/pages/prog/www/WIGOS-WIS/TECO-WIGOS/Conference%20Programme.pdf.

Wehrli C.: NRT Observations in GAW-PFR network, GAW 2009 Meeting, 5-7 May 2009, Geneva. http://www.wmo.int/pages/prog/arep/gaw/GAW_2009_Workshop_materials.html.

Wehrli C.: Wieviel Sonnenstrahlung erträgt oder braucht die Welt, Symposium Klimawandel Apokalypse oder Chance, Academia Raetica, 15. Mai 2009, Chur, Switzerland. http://www.academiaraetica.ch/symposien/seiten/abstracts_klimawandel-09.pdf.

Wuttke S., Schrems O., Gröbner J., Kreuter A., Blumthaler M.: A new UV Spectroradiometer for the Primary Arctic NDACC Site Ny Alesund, Proc. MOCA 09 Joint Assembly, 19-29 July 2009, Montreal, Canada.

Administration

Personnel Department

Sonja Degli Esposti

By the end of 2009 our institute reached a new record number of employees — 36 people are currently employed. Slowly but surely it's getting crowded in our offices … Fortunately, plans for the renovation of our institute are already far advanced and we are all looking forward to our new offices and laboratories!

In 2009, four new employees were hired: Daniel Lachat started his PhD thesis on June 1st in the project "One century of atmospheric transmission over Davos". Three months later Markus Suter joined the DARA space experiment team. Markus served part of his civilian service conscript at PMOD/WRC, and is now working on the design and construction of the DARA Prototype.

In October, Peter Kiedron from NOAA, Boulder, came to Davos as a visiting scientist for one year. His broad experience in spectroradiometry will help us in designing our new diode array based spectroradiometer system.

Last but not least, Marco Senft, our external IT-Supporter, was temporarily hired to program the new data acquisition for the World Standard Group.

Several civilian service conscripts served their time at PMOD/WRC and supported us in different projects. Our sincere thanks are extended to them all.

Figure 1. Staff photo, taken on September 2009

Scientific Personnel

Prof. Dr. Werner Schmutz	Director, physicist
Dr. Tatiana Egorova	Climate group, meteorologist
Dr. Wolfgang Finsterle	Head WRC-section solar radiometry, physicist
Dr. Julian Gröbner	Head WRC-sections IR radiometry, WORCC and EUVC, physicist
Dr. Gregor Hülsen	EUVC scientist, physicist
Dr. Piotr Kiedron	Visiting scientist, physicist (since 1.10.2009)
Dr. Stephan Nyeki	WORCC scientist, physicist
Dr. Eugene Rozanov	Climate group, scientist, physicist
Dr. Alexander Shapiro	Postdoc, solar physics group, physicist
Dr. Rosaria Simoniello	Postdoc, solar physics group, physicist
Dr. Christoph Wehrli	WORCC scientist, physicist
Markus Suter	Scientist, PRODEX project DARA (since 1.9.2009)
André Fehlmann	PhD student, UNIZH
Daniel Lachat	PhD student, UNIBE (since 1.6.2009)

Uwe Schlifkowitz	PhD student, University Freiburg i.Br.
Micha Schöll	PhD student, ETHZ
Anna Shapiro	PhD student, ETHZ
Stefan Wacker	PhD student, UNIBE
Andrea Büschlen	Internship, University Basel (6.7. until 15.9.2009)

Expert Advisor

Dr. Claus Fröhlich	Physicist

Technical Personnel

Silvio Koller	Head technical department and quality system, Electronic engineer
Daniel Pfiffner	Project leader space experiments, deputy head technical department and quality system, Electronic engineer
Daniel Bühlmann	Technician
Marco Senft	Software developer (since 7.9.2009)
Ricco Soder	Research engineer
Marcel Spescha	Technician
Christian Thomann	Technician
Diego Wasser	Electronic technician
Matthias Müller	Electronics apprentice, 1st/2nd year
Samuel Prochazka	Electronics apprentice, 3rd/4th year

Administration

Sonja Degli Esposti	Head administration/Human Resources
Stephanie Ebert	Administration, book keeping
Nadia Casanova	Administration apprentice, 1st/2nd year

Caretaker

Denise Dicht	General caretaker, cleaning
Regula Dicht	Cleaning, part time
Jutta Jäger	Cleaning, part time
Savina Stark	Cleaning, part time (until 1.3.2009)

Civilian Service Conscripts

Robert Cerny	until 9.3.2009
Lars Konersmann	5.1. – 17.1.2009
Markus Suter	19.1. – 22.5.2009
Andreas Reufer	25.5. – 17.9.2009
David Keller	1.6. – 11.9.2009
Daniel Würsch	7.9. – 12.2.2010
Thomas Niederberger	14.9. – 27.11.2009
Roman Koller	since 30.11.2009

Guided Tours

24.02.2009:	4 persons
28.05.2009:	23 persons
04.06.2009:	18 persons
30.06.2009:	16 persons
08.07.2009:	18 persons
21.08.2009:	12 persons
02.10.2009:	5 persons
03.10.2009:	22 persons
03.11.2009:	15 persons
12.11.2009:	15 persons
26.11.2009:	25 persons
09.12.2009:	40 persons

Public Seminars

22.04.2009	Daniel Lachat, Fernerkundung von urbanen Aerosolen mittels LIDAR Ceilometer
27.04.2009	Igor Mokhov, Institute of Atmospheric Physics, Russia, Diagnostics and Modelling of Natural and Anthropogenic Climate Change Effects
27.04.2009	Nikolai F. Elansky, Institute of Atmospheric Physics, Russia, Atmospheric Composition Observations over Russia: TROICA Experiments
07.05.2009	Prof. Dr. Oskar von der Lühe, Kiepenheuer-Institut für Sonnenphysik, Deutschland, Gregor – a New 1.5 m Solar Telescope
08.05.2009	Ramineh Gyr, Gromov-hyperbolic spaces and their characteristics
11.05.2009	Peter Kiedron, NOAA, USA, Notes On Array Spectroradiometers: Rotating Shadowband Spectroradiometers (RSS)
19.05.2009	Upcoming Calls Space and Environment: Euresearch Information Day
14.08.2009	Lucia Kleint, Institute of Astronomy, ETH Zürich, Turbulent Magnetic Fields – Cyclic Variations?
05.09.2009	Weiterbildung “Astronomie”, Mittelschulen ZHSF

Course of Lectures, Participation in Commissions

Werner Schmutz	Course of lecture Astronomie, HS 2009, ETH-ZH Examination expert in astronomy, BSc ETH-ZH Executive board of the International Radiation Commission (IRS, IAMAS) Comité consultatif de photométrie et radiométrie (CCPR, OICM WMO) Expert Team on Meteorological Radiation and Atmospheric Composition Measurements (CIMO, WMO) Committee on Space Research, Commission of SCNAT Executive board of the Swiss Society Astronomy Astrophysics (SSAA), SCNAT GAW-CH working group (MeteoSwiss) Swiss management committee delegate to the COST action ES0803 (ECF)
Wolfgang Finsterle	Expert Team on Meteorological Radiation and Atmospheric Composition Measurements (CIMO, WMO)
Julian Gröbner	Course of Lecture Solar Ultraviolet Radiation HS 2009, ETH-ZH GAW-CH Working group (MeteoSwiss) Swiss management committee delegate to the COST action 726 (ECF) Working group leader of COST action 726 NEWRAD Scientific committee member Working group of Baseline Surface Radiation Network (BSRN) Member of the International Radiation Commission (IRS, IAMAS)
Eugene Rozanov	Member of the International Commission on the Middle Atmosphere (ICMA, IAMAS)
Christoph Wehrli	GAW-CH Working group (MeteoSwiss) Scientific Advisory Group Aerosol (WMO/GAW) SAG sub group AOD, chairman (WMO/GAW) Working group Baseline Surface Radiation Network (WMO/WCRP)

Remission of Debts

The former PMOD/WRC pension plan was indebted over the long-term which dates back to the time when the government paid no contributions into the pension fund. When PUBLICA, which is now in charge of federal pensions, took over from the Pensionskasse des Bundes (PKB), this debt became due for payment and as a result our reserves would have been considerably reduced. A request for acquittal was made to the federal government and we were informed last year that the outstanding debt would be covered. This has allowed the transfer of CHF 265’375.00 from the deferred assets to our reserves. We intend to invest this amount in infrastructure improvements after the major renovation of the PMOD/WRC building has been completed. We thank the federal government for this generous support.

Upgrading and Renovation of the Old Schoolhouse

Werner Schmutz

Considerable funds were invested by the Bundesamt für Bauten und Logistik to construct an emergency exit. This investment was only covered by federal funds and not shared between the three parties who support the operational service of the World Radiation Center. We thank the Swiss government for this generous support.

Back in 1999, when I joined the PMOD/WRC, the staff level was about half of the 36 people that are employed currently at the observatory. This expansion has filled the available space in the Old Schoolhouse and two years ago we started to address the renovation and expansion of the observatory's interior structure. The planning, by a consortium lead by Emch+Berger AG, has now progressed to a proposal which was submitted to the Davos Local Council in order to obtain planning permission. The plans mostly include extensive internal renovation. Most importantly the Observatory will be extended to the fourth floor and new space available to us will comprise an additional optics laboratory, a larger seminar room, and offices for about ten additional people. Special care was taken to minimize any modification of the exterior of the building as the Observatory is a historical landmark of Davos. The only noticeable alteration will be on the north façade, which faces away from Davos town; i.e. the characteristic south façade will remain untouched. This sympathetic design was proposed by the architects Schumacher AG. The costs of the whole project will be fully covered by federal funds, and construction work is scheduled to begin just after the 11th International Pyrheliometer Comparisons in October 2010.

Figure 1. The newly built emergency exit on the west side of the Old Schoolhouse. A new elevator has also been integrated into the structure. Together with an access road behind the mechanical workshop this allows stair-free access of heavy equipment to all floors.

Figure 2. Photo-montage of the south façade illustrating planned alterations of the Old Schoolhouse. Left picture: South façade of the building facing Davos town. No modifications of the main building will occur. Thermal solar cells will be mounted facing south-eastwards (left in the picture), and hardly visible, just behind the solar cells, a new bicycle shed will be installed. Right picture: The north façade of the building. The new addition is the attic extension which is seen on the outside with three windows on the fourth floor. The newly built emergency exit is not included in this photo montage.

Bilanz 2009 inklusive Drittmittel

Aktiven	31.12.2009 CHF
Flüssige Mittel/Wertschriften	1‘432‘024.67
Forderungen	185‘678.10
Aktive Rechnungsabgrenzungen	199‘781.44
	1‘817‘484.21

Passiven	
Verbindlichkeiten	111‘296.00
Kontokorrent Stiftung/SIAF	72‘599.15
Passive Rechnungsabgrenzungen	480‘148.27
Rückstellungen	976‘740.20
Eigenkapital	176‘700.59
	1‘817‘484.21

Erfolgsrechnung 2009 inklusive Drittmittel

	31.12.2009 CHF
Ertrag	
Beitrag Bund Betrieb WRC, IRC, WORCC	1‘307‘186.00
Beitrag Kanton Graubünden	213‘959.00
Beitrag Landschaft Davos Gemeinde	555‘470.00
Beitrag Landschaft Davos Gemeinde, Mieterlass	149‘317.00
Beitrag Bund (BBL) Bau Fluchttreppe/Lift	604‘980.00
Beitrag GAW/CH für EUVC	161‘760.00
Drittmittel	1‘089‘183.41
Forschungsbeitrag EUSAAR	27‘365.65
Beitrag SOTERIA	38‘182.00
Overhead SNF	11‘204.00
Instrumentenverkäufe	236‘587.55
Kalibrationen/Übriger Ertrag	204‘949.90
Finanzertrag	34‘557.45
Schulderlass Bund, Fehlbetrag PKB	265‘375.00
	4‘900‘076.96

	CHF
Aufwand	
Personalaufwand	2‘233‘607.10
Drittmittel	1‘089‘183.41
Investitionen	410‘815.04
Unterhalt	29‘615.90
Verbrauchsmaterial	58‘307.80
Verbrauch Commercial	81‘377.35
Reisen, Kongresse, Kurse	77‘253.90
Bibliothek und Literatur	20‘447.60
Raumaufwand	209‘690.70
Verwaltungsaufwand	53‘986.95
Finanzaufwand	7‘126.57
Übriger Betriebsaufwand	19‘727.00
Bau Fluchttreppe/Lift	604‘980.00
	4‘896‘119.32
Ergebnis 2009	3‘957.64
	4‘900‘076.96

Abbreviations

AEMET	Agencia Estatal de Meteorogia, Madrid, E
AERONET	Aerosol Robotic Network, GSFC
AOD	Aerosol Optical Depth
ASRB	Alpine Surface Radiation Budget
BIPM	Bureau International des Poids et Mesures, Paris, F
BISON	Birmingham Solar Oscillation Network
BOLD	Blind to Optical Light Detector
BOS	Bolometric Sensor, Belgium instrument on the mission PICARD
BSRN	Baseline Surface Radiation Network of the WCRP
BUSOC	Belgian User Support and Operation Centre of ESA
CCM	Chemistry-Climate Model
CAS	Commission for Atmospheric Sciences, Commission of WMO
CCPR	Comité Consultatif de Photométrie et Radiométrie, BIPM
CIE	Commission Internationale de l'Eclairage
CIPM	Comité International des Poids et Mesures
CIMO	Commission for Instruments and Methods of Observation of WMO, Geneva
CMC	Calibration and Measurement Capabilities
CNES	Centre National d'Etudes Spatiales, Paris, F
CNRS	Centre National de la Recherche Scientifique, Service d`Aéronomie Paris
CoI	Co-Investigator of an Experiment/Instrument/Project
COSI	Code for Solar Irradiance – Solar Atmosphere Radiation Transport Code developed at PMOD/WRC
COSPAR	Commission of Space Application and Research of ICSU, Paris, F
CPD	Coarse Pointing Device
CSAR	Cyrogenic Solar Absolute Radiometer
CTM	Chemical Transport Model
CUCF	Central UV Calibration Facility, NOAA, Boulder, USA
DIARAD	Dual Irradiance Absolute Radiometer of IRMB
DLR	Deutsche Luft und Raumfahrt
ESA	European Space Agency, Paris, F
ESF	European Science Foundation
ESTEC	European Space Research and Technology Center, Noordwijk, NL
ETH	Eidgenössische Technische Hochschule (Z: Zürich, L: Lausanne)
EURECA	European Retrievable Carrier, flown August 1992 - June 1993 with SOVA Experiment of PMOD/WRC
EUSAAR	FP6 project: European Supersites for Atmospheric Aerosol Research
EUV	Extreme Ultraviolet Radiation
EUVC	European Ultraviolet Calibration Center at PMOD/WRC
FMI	Finnish Meteorological Institute
FP6/FP7	European Framework Program of the European Commission
FRC-II	Filter Radiometer Comparison II
GAW	Global Atmosphere Watch, an Observational Program of WMO
GAWTEX	GAW Training & Education Center
GCM	General Circulation Model
GHG	Greenhouse Gases
GOLF	Global Oscillations at Low Frequencies, Experiment on SOHO
GSFC	Goddard Space Flight Center, Greenbelt, MD, USA
IACETH	Institute for Climate Research of the ETHZ
IAMAS	International Association of Meteorology and Atmospheric Sciences of IUGG
IAU	International Astronomical Union of ICSU, Paris, F
ICSU	International Council of Scientific Unions, Paris, F
IPC	International Pyrheliometer Comparisons
IR	Infrared
IRC	International Radiation Commission, Commission of IAMAS
IRIS	Infrared Integrating Sphere Radiometer
IRMB	Institut Royal Météorologique de Belgique, Brussel, B
IRS	International Radiation Symposium of the Radiation Commission of IAMAS
ISO/IEC	International Oranisation for Standardization/International Electrotechnical Commission
ISS	International Space Station
IUGG	International Union of Geodesy and Geophysics of ISCU
JRC	Joint Research Center of the European Commission in Ispra, I
KIS	Kiepenheuer-Institut für Sonnenphysik, Freiburg i.Br., D
LATMOS	Laboratoire Atmosphères, Milieux, Observations Spatiales, French research institution
LYRA	Lyman-alpha Radiometer, PMOD/WRC Experiment on PROBA 2
METAS	Federal Office of Metrology
MGO	Main Geophysical Observatory, St. Petersburg, RUS
MITRA	Monitor to Determine the Integrated Transmittance
NASA	National Aeronautics and Space Administration, Washington DC, USA
NEWRAD	New Developments and Applications in Optical Radiometry
NILU	Norwegian Institute for Air Research
NIST	National Institute of Standards and Technology, Gaithersburg, MD, USA
NOAA	National Oceanographic and Atmospheric Administration, Washington DC, USA
NPL	National Physical Laboratory, Teddington, UK
NRL	Naval Research Laboratory, Washington DC, USA
NREL	National Renewable Energy Lab, Golden, CO, USA
NRT	Near Real Time
ODS	Ozone Destroying Substances
PFR	Precision Filter Radiometer
PI	Principle Investigator, Leader of an Experiment/Instrument/Project
PICARD	French Space Experiment to Measure the Solar Diameter, to be launched 2010
PMOD	Physikalisch-Meteorologisches Observatorium Davos
PMO6	PMO6 Type Radiometer
PREMOS	Precision Monitoring of Solar Variability, PMOD/WRC Experiment on PICARD, to be launched 2010
PROBA 2	ESA Technology Demonstration Space Mission, launched 2 December 2009
PRODEX	Program for the Development of Experiments, ESA
PTB	Physikalisch-Technische Bundesanstalt, Braunschweig & Berlin, D
QASUME	Quality Assurance of Spectral Ultraviolet Measurements in Europe
QMS	Quality Management System
RA	Regional Association of WMO
SCNAT	Swiss Academy of Sciences
SCOPES	Scientific Collaboration between Eastern Europe and Switzerland, Grant of the SNSF
SLF	Schnee und Lawinenforschungsinstitut, Davos
SFI	Schweiz. Forschungsinstitut für Hochgebirgsklima und Medizin, Davos
SI	International System of Units
SIAF	Schweiz. Institut für Allergie- und Asthma-Forschung, Davos
SMHI	Swedish Meteorological and Hydrological Institute
SNSF	Swiss National Science Foundation
SOCOL	Combined GCM and CTM Computer Model, developed at PMOD/WRC
SOHO	Solar and Heliospheric Observatory, Space Mission of ESA/NASA
SOLAR	Experiment Platform on the ISS
SORCE	Space Mission of NASA
SOTERIA	Solar-Terrestrial Investigations and Archives
SOVA	Solar Variability Experiment on EURECA
SOVIM	Solar Variability and Irradiance Monitoring, PMOD/WRC Experiment on the International Space Station Alpha, 2008
STEP	Solar Terrestrial Energy Program of SCOSTEP/ICSU
SUSIM	Solar Ultraviolet Spectral Irradiance Monitor on Board UARS
UARS	Upper Atmosphere Research Satellite of NASA
UV	Ultraviolet
UVA	UV Radiation in the Range of 315-400 nm
UVB	UV Radiation in the Range of 280-315 nm
VIRGO	Variability of Solar Irradiance and Gravity Oscillations, PMOD/WRC Experiment on SOHO, launched December 1995
WCRP	World Climate Research Program
WDCA	World Data Center for Aerosols, Ispra, I
WIGOS	WMO Integrated Global Observing System
WIS	WMO Information System
WISG	World Infrared Standard Group of Pyrgeometer, maintained by WRC
WMO	World Meteorological Organization, a United Nations Specialized Agency, Geneva
WRC	World Radiation Center, Davos
WRC-IRS	Infrared Radiometry Section of WRC
WRC-SRS	Solar Radiometry Section of WRC
WRC-WORCC	World Optical Depth Research and Calibration Center, WRC Section
WRDC	World Radiation Data Center, St. Petersburg, RUS
WRR	World Radiometric Reference
WSG	World Standard Group, realizing the WRR, maintained by WRC
WWW	World Weather Watch, an Observational Program of WMO

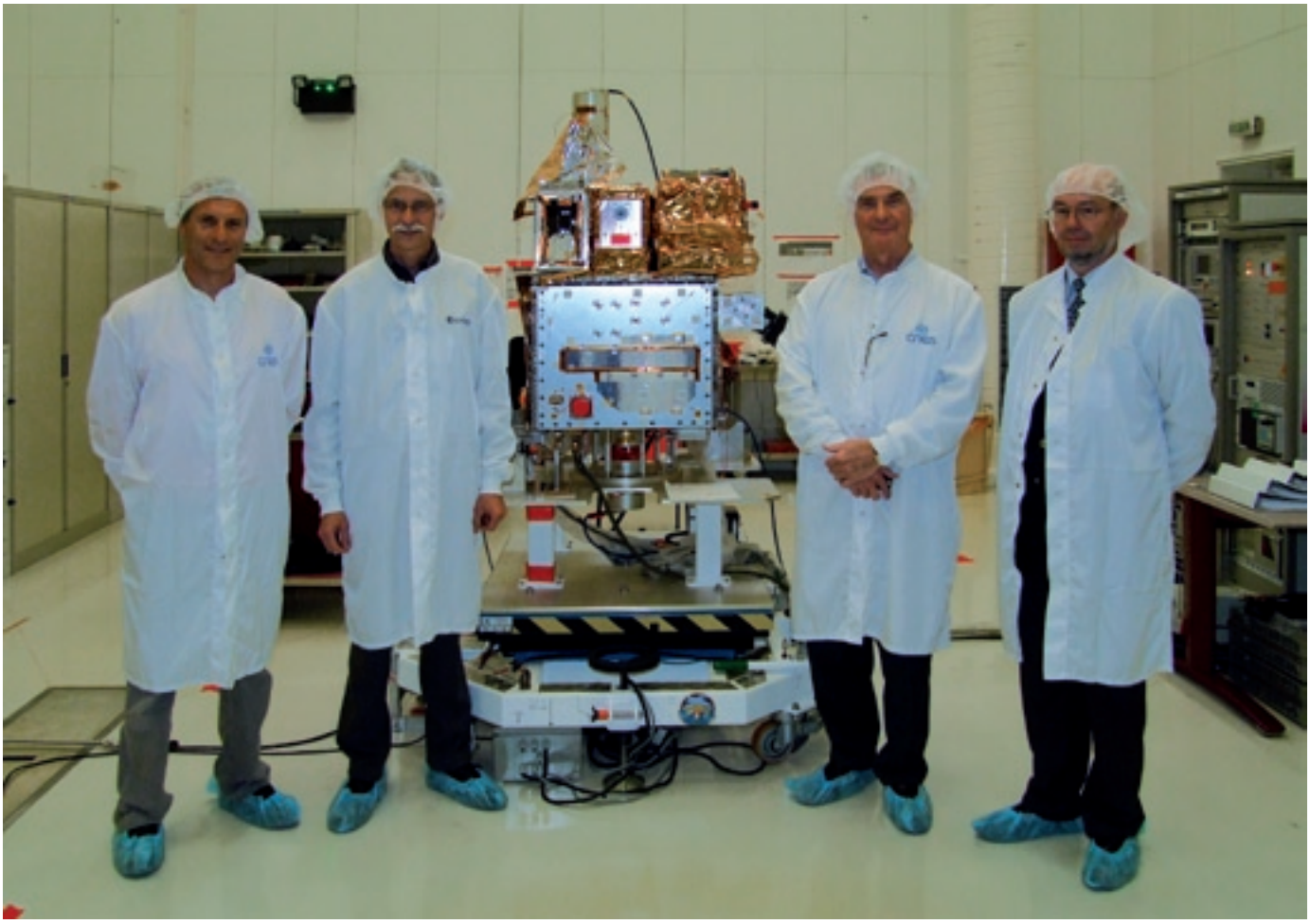

Figure 1. Visit to the CNES laboratories at Toulouse during the PICARD Science Committee meeting on October 22, 2009. The satellite PICARD is finally fully-assembled with the science experiments PREMOS, SOVAP, BOS, and SODISM (from left to right). Persons from left to right are: the PICARD project manager, François Buisson, CNES France; PREMOS PI Werner Schmutz, PMOD/WRC Switzerland: PICARD PI and SODISM PI Gérard Thuillier, LATMOS France; BOS PI Michel van Ruymbeke, ROB Belgium. Missing on this photograph is the SOVAP PI Steven Dewitte, ROB, Belgium.

Figure 2. Close-up view of PREMOS (left) and SOVAP / BOS (right) experiments. The front of PREMOS is covered with highly reflective back surface mirrors with round viewing holes for the filter radiometer instruments (two 2x2 groups) and the absolute radiometer instruments (two holes at the bottom; Photo: M. van Ruymbeke).

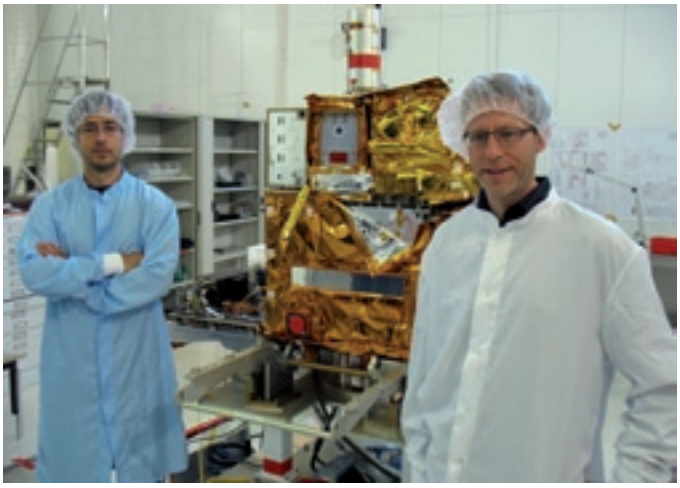

Figure 3. The PREMOS project manager Daniel Pfiffner (left) and the head of PMOD/WRC technical department Silvio Koller (right) in front of PICARD. The picture was taken after the integration of PREMOS on PICARD on August 18, 2009 at CNES Toulouse.

Dorfstrasse 33, 7260 Davos Dorf, Switzerland
Phone +41 81 417 51 11, Fax +41 81 417 51 00
www.pmodwrc.ch